## Contents

# MECHANISMS OF LIPOSOMAL CONTRAST AGENTS IN MAGNETIC RESONANCE IMAGING

B. Pütz[1,3], D. Barsky⋆[2,3] and Klaus Schulten[1,2,3]
[1]Department of Physics, [2]Program in Biophysics, and [3]Beckman Institute
University of Illinois at Urbana-Champaign
405 N. Mathews Avenue, Urbana, Illinois 61801

**ABSTRACT**

We review the mechanisms by which liposomal contrast agents—solutions of liposomes that entrap and deliver (usually paramagnetic) contrast agent into specific tissues—cause a desired enhancement of the bulk relaxation rate in tissues. The relaxation-enhancing action for transverse magnetization can be most generally explained by exchange (inner sphere relaxation) and diffusional dephasing (outer sphere relaxation). Simple analytic expressions for inner and outer sphere relaxation mechanisms are presented. At typical MRI field strengths ($\gtrsim 1\,$T) longitudinal magnetization is affected only by inner sphere relaxation. For typical liposomal preparations the transverse magnetization relaxation is also dominated by the inner sphere mechanism. For rather low effective concentrations (2 mM) of $\mathrm{Gd(DTPA)}^{2-}$, a relaxation rate enhancement of several Hertz is typically achieved, and the rate increases linearly with the concentration of liposomes. The inner sphere model presented here is similar to recent descriptions which significantly generalize earlier models which have not taken into account the finite lifetime of water inside the liposomes. The present model describes how the permeability, the relative size and the relaxivity of the entrapped contrast agent affect the bulk relaxivity of the tissue to which liposomal contrast agents have been introduced. Outer sphere relaxation plays a minor role and is comparable to inner sphere relaxation only for larger (diameters $\gtrsim 500\,$nm), reasonably impermeable ($P_d \lesssim 10^{-3}\,$cm/s) liposomes for which the bulk rate enhancement is rather low—about one Hertz. A notable exception occurs for giant (diameters $\sim 10\,\mu$m), multivesicular liposomes where the bulk rates can be many times higher. Simulations have been carried out for the purpose of investigating the simultaneous action of inner and outer sphere relaxation. The simulations reveal the expected dependence of outer sphere relaxation time on the echo time, but they consistently predict a relaxation rate about twice as high as what the outer sphere theory predicts. In the realm of liposomes studied here, the simulations imply an independence of the inner and outer sphere relaxation mechanisms; i. e., relaxation enhancements can be calculated independently and simply added.

# 1 Introduction

For some applications of magnetic resonance imaging (MRI), image contrast can be enhanced through MRI contrast agents, paramagnetic molecules or superparamagnetic substances which increase signal relaxation rates in specific tissues. This review examines the mechanisms by which liposomal contrast agents, i. e., solutions of liposomes that entrap and deliver paramagnetic molecules, cause an enhancement of the bulk water relaxation rate in tissue.

An understanding of the enhancement of water relaxation is pertinent to the design of liposomal contrast agents and to the interpretation of their effects in images. For example, to reach the usual goal of achieving the highest relaxation enhancement liposomes should generally be made as small as possible. A high permeability of the liposomal membrane and a high entrapped concentration of the agent will also increase relaxation rates. A simple formula, presented below, relates these physical parameters to relaxation rates. It allows one to predict, for example, by how much the concentration of contrast agent should be increased to double a relaxation rate. This tool should be highly useful in diagnostic imaging where the physical parameters are constrained by temperature, toxicity, tissue absorbance, or other factors.

For general studies of membrane activity as well as for purposes of designing liposomal contrast agents, the reliable characterization of membrane permeability is of fundamental importance. While this has been standardly accomplished by the use of paramagnetic contrast agents [1, 2, 3], the interpretation presented here of how the bulk relaxation rate reflects the membrane permeability has been significantly generalized from earlier models to include the finite relaxivity of the entrapped agent and the finite residence time of the water inside the liposomes.

Simple, unilamellar liposomes consist of a lipid bilayer shell which encloses an aqueous compartment. There are currently two widely considered types of liposomal contrast agents: those that entrap a solution of paramagnetic molecules in the aqueous compartment and those that incorporate the paramagnetic molecules in the liposomal membrane, by either covalent bonds to the acyl chain of the lipids or by chelation to a ligand which is itself incorporated into the membrane. Elsewhere in the present Forum, Unger and coworkers have suggested the terms "ensomes" (entrapped agents) and "memsomes" (membrane-incorporated agents) for the two types, respectively. Ensomes, in fact, may themselves be divided into two categories: those that are designed to release a paramagnetic agent within particular tissues, and those that continue to entrap a paramagnetic agent even as they effect an enhanced relaxation of the surrounding water.

Although studies and trials with ensomes have predated those involving memsomes, there is currently some preference towards the latter for the following reasons [4, 5]. First, although the smallest ensomes provide the highest relaxivity, their trapping efficiency is worst—in terms of both the agent to lipid ratio of each liposome and the ratio of entrapped agent to that which must be washed away. Secondly, ensomal relaxivity is normally less than that of the entrapped contrast agent because water must exchange across the liposomal membrane. Liposomal stability, i. e., full containment of the paramagnetic agent, is also at odds with the need to heighten the permeability of the membranes to water in order to achieve maximal relaxivity. What is more, because in memsomes the paramagnetic ions are bound to ligands, the ions have a much longer rotational correlation time and therefore have a greater relaxivity (per mole) than they have in solution. Finally, if the paramagnetic ion-ligand complex flows freely over the membrane surface, then the size of the liposome has no effect of the relaxivity of the contrast agent [5].

Nevertheless, there are still many reasons to employ ensomes and understand the mechanisms by which they cause relaxation. Both ensomes and memsomes will provide similar site specific distribution; i. e., they will be absorbed primarily by macrophage-rich tissue. Ensomes, however, protect the contrast agent from binding to plasma proteins and the provide the possibility of controlling water access [4, 6, 7, 8].[1] It is of great practical importance that both $Gd(DTPA)^{2-}$ and liposomes are (at least separately) currently in clinical use, while memsomal compounds such as the lipophilic chelates of Gd may be slow in gaining clinical approval. Moreover, ensomes are biologically more interesting in that they provide a simple model of cells and compartmentalized tissues, examples of which include Kupffer cells of the liver [9], erythrocytes [10, 11, 12, 13], and capillaries [14]. Finally, only ensomes will produce an additional $T_2$ (outer sphere) relaxation effect, a point which will be developed later.

In the present review we consider a paramagnetic contrast agent, e. g., Gd-$(DTPA)^{2-}$ [15, 16], which is fully entrapped by liposomes in solution. Such ensomes have been successfully used in animals to improve MRI contrast between normal liver and tumors [17, 18, 19]. Although the authors know of no trials to date of liposomal contrast agents in humans, liposomes are already in use as drug delivery agents [20]. In comparing the models presented here with published data, we consider only $Gd(DTPA)^{2-}$-filled liposomes, although $Mn^{2+}$-filled liposomes are also being developed and should behave similarly, with the added feature that $Mn^{2+}$ may bind to lipids and thereby increase its relaxivity [21].

An especially complete description of relaxation enhancement due to paramagnetic molecules and superparamagnetic particles has been provided by Gillis and Koenig [10]. Concerning paramagnetic molecules, we note the following points. First, both longitudinal and transverse relaxation rates (characterized by $T_1$ and $T_2$, respectively) of water protons are nearly equally affected by the addition of paramagnetic molecules to the water. Second, the relaxation enhancement comes about by short-ranged interactions ("collisions") between water molecules and paramagnetic molecules [10, 22]. There is also a "secular" transverse relaxation which accounts for the dephasing of nuclear magnetization while diffusing in the presence of magnetic field inhomogeneities. For paramagnetic molecules added directly to water, this effect is negligible. Yet, in the vicinity of much larger particles such as liposomes ($\gtrsim$

50 nm) containing paramagnetic molecules, this can be a measurable effect.

These considerations will now be applied to liposomal systems. For appropriately constructed ensomes the contrast agent is strictly confined to the liposome interior [17, 19]. Accordingly, longitudinal relaxation rates $T_1^{-1}$ measured for solutions of $\mathrm{Gd(DTPA)}^{2-}$-filled liposomes can be explained by water proton transport—*exchange*—across the cell membranes [23, 24, 25, 26]. Due to susceptibility differences between liposomes and the surrounding water, such liposomal systems give rise to magnetic dipole fields around the liposomes such that transverse relaxation rates $T_2^{-1}$ are enhanced by *diffusion* around—rather than into—the liposomes. The same effect can occur around biological cells which are generally $10^2$–$10^3$ times larger than liposomes [14]. Exchange alone can usually (by adjusting the inferred membrane permeability) account for enhanced rates of transverse relaxation [27]. Nevertheless, the fundamental coexistence of the two mechanisms, *exchange* and *diffusion*, demand that the separate contributions to $T_2$ be singled out. Also, while susceptibility differences between $\mathrm{Gd(DTPA)}^{2-}$-filled liposomes and the surrounding solution should hardly influence the longitudinal relaxation [10], $T_1$-weighted *images* may still be affected by such mechanisms since the transverse relaxation ($T_2$) accompanies nearly all imaging techniques. Stated differently, large enhancements of transverse relaxation are always relevant to diagnostic imaging.

Koenig and coworkers [10, 28, 25] consistently distinguish between "inner sphere" and "outer sphere" relaxation. This useful nomenclature originates from descriptions of inter-molecular relaxation: inner sphere relaxation occurs through binding between the paramagnetic complex and the magnetically excited molecule, while outer sphere relaxation occurs as magnetically excited molecules pass through the magnetic dipolar field distortions (and fluctuations) produced by the paramagnetic complexes. In the context of the liposomal system at hand, inner sphere relaxation refers to relaxation of the water through *exchange*. This mechanism greatly affects the relaxation rate of the bulk since a large fraction of the bulk water exchanges with the liposomal interior(s) during the course of the measurement. Outer sphere relaxation, on the other hand, refers to any additional relaxation due to diffusion of the water through the dipole fields *outside* the liposomes.

In this work we investigate models of both inner and outer sphere mechanisms. The inner sphere models can be described analytically, numerically and through simulation, depending on the level of generality. Outer sphere relaxation can also be modeled analytically—either through quantum mechanics [29] or through a classical model of bounded diffusion in a linear magnetic field gradient [30, 31]. For typical liposomal systems, inner sphere relaxation will be seen to dominate the bulk rate. Both inner sphere and outer sphere relaxation for most cases can be easily calculated by the simple formulas presented here. For very large liposomes (diameter $\gtrsim 500\,\mathrm{nm}$) the outer sphere theory should no longer apply, but one may still make useful estimates or resort to simulation, as has been done for the case of red blood cells [14]. Furthermore, we address through detailed simulation in how far inner sphere and outer sphere relaxation rates are additive.

## 2 Models of Relaxation

We employ several different models to a system of liposomes which entrap a paramagnetic contrast agent in their interior, and which are surrounded by bulk water devoid of contrast agent. These models are, in order of increasing generality: (1) analytic models—a two-compartment model of inner sphere relaxation, and both classical and quantum mechanical models of outer sphere relaxation; (2) a numerical, many-compartment model employing a numerical discretization scheme together with an efficient algorithm known as the generalized moment expansion [32]; and (3) a continuous, random walk model realized by Monte-Carlo simulations.

We begin with a classical description of nuclear spin magnetization developed by Bloch. The local magnetization is an average property of water molecules and is subject to the diffusion of the water molecules. Each component of the local nuclear magnetization $\vec{m}(\vec{r},t)$ is described by the Bloch equations to which a diffusion term $\nabla \cdot D(\vec{r})\nabla$ has been added [33, 34]

$$\partial_t \begin{pmatrix} m_{\mathrm{trans}}(\vec{r},t) \\ m_{\mathrm{long}}(\vec{r},t) \end{pmatrix} = \left[\nabla \cdot D(\vec{r})\nabla - \begin{pmatrix} \mathrm{i}\omega_0 + T_{2,0}^{-1}(\vec{r}) \\ T_{1,0}^{-1}(\vec{r}) \end{pmatrix}\right] \begin{pmatrix} m_{\mathrm{trans}}(\vec{r},t) \\ m_{\mathrm{long}}(\vec{r},t) \end{pmatrix}, \qquad (1)$$

where $D(\vec{r})$ is the local diffusion coefficient of water, $\omega_0$ is the Larmor frequency, and $T_{2,0}^{-1}(\vec{r}), T_{1,0}^{-1}(\vec{r})$ are the local transverse and longitudinal native relaxation rates. The spatial dependence of these rates will be simple radial step functions of the short and long relaxation times in the presence and absence of a contrast agent, respectively. The second subscript (zero) indicates that $T_{1,0}$ and $T_{2,0}$ are "native" relaxation times, i. e., the times measured in a solution of contrast agent or in plain water in the absence of diffusion or exchange between environments.

If we ignore the effects of magnetic field inhomogeneities, e. g., due to susceptibility differences, we can rewrite Eq. (1) as

$$\partial_t m(\vec{r}, t) = [\mathcal{D}(\vec{r}) - k(\vec{r})]\, m(\vec{r}, t), \tag{2}$$

where $\mathcal{D}(\vec{r}) = \nabla \cdot D(\vec{r})\nabla$, $k(\vec{r}) = T_{1,0}^{-1}(\vec{r})$ or $T_{2,0}^{-1}(\vec{r})$, and $m(\vec{r}, t) = m_{\text{long}}(\vec{r}, t)$ or $m_{\text{trans}}(\vec{r}, t)$.[2] The physical observable is the overall magnetization, $M(t) = \int_\Omega d\Omega m(\vec{r}, t)$ where $d\Omega$ is a differential surface or volume element for two or three dimensional geometries, respectively and the integration is over the whole space. Equation (2) describes inner sphere relaxation well, but cannot describe outer sphere relaxation since the precession term has been factored out.

### 2.1 Two site model—inner sphere relaxation

In water doped with a chelated paramagnetic species, e. g., $\text{Gd(DTPA)}^{2-}$, a nuclear spin must not only diffuse into the immediate vicinity of a paramagnetic molecule in order to experience a faster relaxation of its magnetization, it must also bind at the single coordination site available for the water molecules [35]. Consequently, since the contrast agent is located solely within the liposome interior, we assume here that water protons must enter the interior in order to be relaxed at a rate faster than the native rate. Thus, we consider only the inner sphere relaxation for both longitudinal and transverse relaxation and, for the present, ignore any transverse outer sphere relaxation.

The key factors that give rise to contrast enhancement are those that affect the rate at which an average water molecule can enter a liposome and become relaxed.

These factors are (1) the average size of the liposomes, (2) the number of liposomes per unit volume, (3) the permeability of the liposomal membrane to water, and (4) the relaxivity of the contrast agent inside the liposomes. In liposomal systems these factors can be experimentally controlled; Refs. [17, 3, 36] demonstrate how the mentioned properties change relaxation rates of bulk water.

Recently investigated liposome systems [25, 36] employed the paramagnetic contrast agent $Gd(DTPA)^{2-}$. In water doped with this agent, the relaxation times $T_1$ and $T_2$ are much shorter than in plain water; for example, $T_1$ for water protons in 100 mM $Gd(DTPA)^{2-}$ is about 1000 times shorter than in water, and this factor is nearly a linear function of concentration. Thus, at a 670 mM $Gd(DTPA)^{2-}$ concentration in liposomes one expects extremely short relaxation times (on the order of 0.5 ms) in the liposome interior. In an earlier, one site model [24, 26] we made the simplifying assumption that water protons lose their magnetization immediately after entering the liposome interior. Here we relax that assumption, and assign a finite, empirically derived relaxation rate to the liposome interior as has also been done in [25].

The (bulk) water outside of the liposomes can be parcelled into imaginary cells of equal volume $V$ for each liposome, and one can consider the diffusion of water to be confined to within these cells, i. e., as if the bulk consisted of cells separated by *impenetrable* walls. This situation is physically equivalent to the real, undivided system because the effect on a water molecule visiting two *different* liposomes at times $t_1$ and $t_2$, in practice, cannot be distinguished from the effect of a water molecule visiting the *same* liposome at times $t_1$ and $t_2$. Therefore, we model the entire diffusion space by a small spherical cell, divided into two concentric, spherical regions (Fig. 1): a liposome interior where water spins relax rapidly due to the contrast agent (I) and an outer region (II) that includes the liposomal membrane as well as the surrounding volume according to

$$\frac{V_{\mathrm{I}}}{V_{\mathrm{II}}} = \frac{C_{\mathrm{eff}}}{C_o} = V_f, \tag{3}$$

where $V_{\mathrm{I}}$ and $V_{\mathrm{II}}$ are the respective volumes of regions I and II, and $V_f$ is the fraction of the volume containing contrast agent.[3] This fraction can be experimentally determined as the ratio of the effective Gd(DTPA)$^{2-}$ concentration, $C_{\text{eff}}$, to the concentration inside the liposomes, $C_o$.

Exploiting the spherical symmetry of this system we can employ the simpler, radial forms of Eqs. (1) and (2); i. e., $\vec{r} \to r$ and $\mathcal{D}(\vec{r}) = \nabla \cdot D(\vec{r})\nabla \to \mathcal{D}(r) = \frac{1}{r^2}\partial_r r^2 D(r)\partial_r$. Written in this form, the outer boundary of region II corresponds to a reflective boundary condition

$$\partial_r m(r,t) = 0, \quad \text{at } r = r_3. \tag{4}$$

Nevertheless, here we do not directly solve Eq. (2), but rather we make use of known solutions, derived in [26], to provide us with the exchange rates across the membrane. We then assume that the magnetization can be well described by two components, $m_{\text{i}}$ and $m_{\text{o}}$, corresponding to the overall magnetization (signal amplitude) in each region. A key implicit assumption in this model is that all spins in both regions have equal access to the partition between the regions, or, in other words, the magnetization does not have any spatial dependence within each of the two regions. If we define a "diffusional exploration time," i. e., the order of time it takes one particle to diffuse the distance between two liposomes

$$\tau_D = \frac{r_3^2}{D_w}, \tag{5}$$

where $D_w$ is the diffusion coefficient of water, then for this assumption to be valid $\tau_D$ should be much shorter than the membrane-exchange time. For a volume fraction of 0.003, $\tau_D$ ranges from about 19 $\mu$s for 70 nm liposomes to 790 $\mu$s for 400 nm liposomes—all much shorter times than the membrane exchange time.

Factoring out the native relaxation[4], the magnetization of the system can be described by a system of two coupled ordinary differential equations

$$\frac{d}{dt}\begin{pmatrix} m_{\text{i}}(t) \\ m_{\text{o}}(t) \end{pmatrix} = \underbrace{\begin{pmatrix} -(R_{\text{i}} + R_{\text{io}}) & R_{\text{oi}} \\ R_{\text{io}} & -R_{\text{oi}} \end{pmatrix}}_{\mathcal{R}} \begin{pmatrix} m_{\text{i}}(t) \\ m_{\text{o}}(t) \end{pmatrix}, \tag{6}$$

where $m_\mathrm{i}(t)$ and $m_\mathrm{o}(t)$ are the magnetization inside the liposome (region I) and outside (region II), respectively. The rate matrix $\mathcal{R}$ consists of $R_\mathrm{i} = T_\mathrm{i}^{-1}$, the relaxation rate caused by the agent inside the liposome, and the two exchange rates $R_\mathrm{io}$ and $R_\mathrm{oi}$; $R_\mathrm{oi}$ is the rate of water molecules passing from outside the liposome (region II) to inside (region I), and $R_\mathrm{io}$ is the rate of transport in the opposite direction (see Fig. 1). Initially, the total magnetization $m_\mathrm{i}(0) + m_\mathrm{o}(0)$ is normalized to unity and it holds $m_\mathrm{i}(0)/m_\mathrm{o}(0) = V_f$.

The description according to Eq. (6) leads to a bi-exponential time dependence for the total magnetization where the two rates are given by the eigenvalues of $\mathcal{R}$. The eigenvalues are distinct (non-degenerate) as long as the membrane is not infinitely permeable. An infinitely permeable membrane would correspond to a fast exchange condition, and in that case the single eigenvalue would be the weighted average of the two rates $R_\mathrm{native}$ and $R_\mathrm{i}$. When the eigenvalues are distinct, the resulting eigenvectors describe two new components of the magnetization $m_\mathrm{fast}(t)$ and $m_\mathrm{slow}(t)$. The amplitude of the fast component $m_\mathrm{fast}$ is much smaller than that of $m_\mathrm{slow}$ as long as $V_f$ is small, and $m_\mathrm{fast}(t)$ relaxes on a time scale that is usually not observed ($\leq$ ms). Hence the bulk signal relaxation enhancement is described almost completely by $m_\mathrm{slow}$. Its corresponding relaxation rate is given by

$$R_\mathrm{slow} = \frac{(R_\mathrm{io} + R_\mathrm{oi} + R_\mathrm{i}) - \sqrt{(R_\mathrm{io} + R_\mathrm{oi} + R_\mathrm{i})^2 - 4R_\mathrm{oi}R_\mathrm{i}}}{2}. \tag{7}$$

Including only the first two terms of the Taylor expansion of the square root around $(R_\mathrm{io} + R_\mathrm{oi} + R_\mathrm{i})^2$ this expression simplifies to

$$R_\mathrm{slow} = \frac{R_\mathrm{oi}R_\mathrm{i}}{R_\mathrm{io} + R_\mathrm{oi} + R_\mathrm{i}} + \frac{(R_\mathrm{oi}R_\mathrm{i})^2}{(R_\mathrm{io} + R_\mathrm{oi} + R_\mathrm{i})^3} \ . \tag{8}$$

For typical parameters (see below) the second term is usually negligible compared to the first.

Since the molecular diffusion is in equilibrium, i. e.,

$$R_\mathrm{oi} = V_f R_\mathrm{io}, \tag{9}$$

the particle density should remain constant even as water molecules exchange across the membrane. Using relation (9), one can express (8) as

$$\frac{1}{T_{\text{para}}} \equiv R_{\text{slow}} = \frac{V_f R_{\text{io}} R_{\text{i}}}{R_{\text{io}}(1+V_f)+R_{\text{i}}} \overset{V_f \ll 1}{\simeq} \frac{V_f R_{\text{io}} R_{\text{i}}}{R_{\text{io}}+R_{\text{i}}} \equiv \frac{V_f \tau_{\text{io}}^{-1} T_{\text{i}}^{-1}}{\tau_{\text{io}}^{-1}+T_{\text{i}}^{-1}} = \frac{V_f}{\tau_{\text{io}}+T_{\text{i}}}. \quad (10)$$

which is identical to the results of Swift and Connick [37] that Koenig [25] employs. The time $T_{\text{para}}$ measures the decrease of the relaxation time with respect to the native relaxation time $T_0$, and it holds

$$\frac{1}{T_{\text{para}}} = \frac{1}{T_{\text{observed}}} - \frac{1}{T_0}, \quad (11)$$

where $T_{\text{observed}}$ is the relaxation (slow component) actually observed.

The times $T_{\text{observed}}$, $T_0$, and $T_{\text{i}}$ can be measured experimentally and, through Eq. (10), the lifetime of water molecules inside the liposome, $\tau_{\text{io}}$, can be determined. If one relates $\tau_{\text{io}}$ to the membrane permeability, one can, through (10), derive the permeability from a measurement of the relaxation rates. In [25] the exchange time $\tau_{\text{io}}$ has been related to the membrane permeability $P_d$ as follows

$$\tau_{\text{io}} = \frac{V}{P_d S} = \frac{r_1}{3P_d}, \quad (12)$$

where $r_1$ is the *inside* radius of the liposome (see Fig. 1). The permeability can thus by determined using

$$P_d = \frac{r_1}{3(V_f T_{\text{para}} - T_{\text{i}})}. \quad (13)$$

**Membrane transit included** Equation (12) does not, however, accurately describe the lifetime of water molecules in the interior of the liposome, i. e., the time the water molecules are exposed to the contrast agent, but rather, it describes the escape of water molecules across the membrane of liposomes with *outer* radius $r_1$ (with inner radius $r_1 - d$, where $d$ is the membrane thickness) [26]. The point is that if molecules are in transit within the membrane, they are neither "out," nor are they still in region I where they would be exposed to the contrast agent. The two associated issues are (1) how long do spins typically reside in the membrane and (2) to what extent are they protected from the $Gd(DTPA)^{2-}$ while inside the membrane? The second question is related to whether the contrast agent can penetrate the lipid bilayer. Koenig et al. point out that since $Mn^{2+}$ interacts with the interfacial charged groups, the same may hold for $Gd(DTPA)^{2-}$ [21, 25]. Concerning the first question, a detailed model of water transport across liposomal membranes is still not available, so we cannot know exactly how much of the exchange time $\tau_{\rm io}$ is spent in the membrane. Here Koenig et al. suggest that since the activation enthalpy for water transport does not change very much between liposomal systems of between zero and 30% cholesterol, and yet cholesterol is observed to cause an increase in the local orientational order within the lipid acyl chains, it is the penetration of the head group region and not the transport through the whole bilayer that limits the exchange. Even so, to better describe the situation where water molecules only have to get into the membrane to experience the native (slow) relaxation rate, we use the time it takes particles to reach the inside of a liposome [26],

$$\tau_{\rm oi} = \frac{r_3^3}{3P_d r_1 r_2}, \tag{14}$$

together with the equilibrium relation (9), to calculate

$$\tau_{\rm io} = \frac{r_1^2}{3P_d r_2} = \frac{r_1\, d}{3D_{\rm m}} \left(\frac{r_1}{r_1 + d}\right). \tag{15}$$

Here $r_2$ is the *outside* radius of the liposome, $r_3$ is the radius of the average volume per liposome, $d = r_2 - r_1$ is the membrane thickness, and $D_{\rm m} = P_d\, d$ is the diffusion coefficient of water in the membrane (cf. Fig. 1). We thus find a new expression for the membrane permeability

$$P_d = \frac{r_1^2}{3r_2(V_f T_{\rm para} - T_{\rm i})}, \tag{16}$$

which is reduced by a factor $r_1/r_2$ compared to Eq. (13). This modification is minor for larger liposomes, but for 50 nm (outer diameter) liposomes it reduces $P_d$ by 20 %.

For applications of liposomes to imaging, one typically would like to know the activity of a liposomal system for a given membrane composition. Solving Eq. (16) for $1/T_{\mathrm{para}}$, one obtains

$$1/T_{\mathrm{para}} = \frac{V_f}{T_i + {r_1}^2/3P_d r_2}. \tag{17}$$

**Water displaced by contrast agent** When large salts such as $Na_2Gd(DTPA)$ are disolved in water, some fraction of water will be displaced by the ions. This will have the effect of reducing $V_f$ in the formulas presented above by exactly the fraction of water displaced, but will not affect the radii. For a 100 mM concentration of $Gd(DTPA)^{2-}$, approximately 17% of the water volume is taken up by the ions (cf. Appendix) [38]. Thus, $1/T_{\mathrm{para}}$ will be reduced by 17% (cf. Eq. 17). This effect, however, acts oppositely to the effect of the membrane thickness. A specific example is provided below in Results.

## 2.2 Discrete shell approximation

It is straightforward to solve the radial form of Eq. (2) by numerical methods. Numerical integration is necessary since it is not possible to integrate analytically the Bloch-diffusion equation for spatially inhomogeneous relaxation rates. This solution serves as a check on some of the assumptions in the former model. Although the two-site model describes the exchange aspect of most liposomal systems quite well, this success depends (1) on the high diffusion constant of the solvent (water) and (2) on a sufficiently high volume fraction $V_f$. If either were to become so low that the diffusional exploration time $\tau_D$ became comparable to the membrane-exchange time, then the two-site model would no longer give accurate results.

To obtain a solution in the form of a sum of exponential decays, we employ the generalized moment expansion [32]. We first make a finite difference approximation to the radial form of Eq. (2), whereby the diffusion space is discretized and, by the spherical symmetry, mapped onto a $1 \times N$ lattice whose sites correspond to discrete shells of the spherical diffusion space. The Brownian motion of the water protons is represented by jumps between adjacent lattice shells. The "jumps" are described by an $N \times N$, tridiagonal transition matrix $\mathbf{D}$ which replaces the differential diffusion operator $\mathcal{D}(r)$ [32, 39]. Similarly, the scalar reaction operator $k(r)$, defined by Eq. (2), is mapped onto a diagonal matrix $\mathbf{K}$ with elements $K_{nn} = k(r = r_n)$. With this notation the master equation corresponding to Eq. (2), i. e., the finite difference approximation to Eq. (2), can be written as follows

$$\partial_t \mathbf{m}(t) = [\mathbf{D} - \mathbf{K}]\, \mathbf{m}(t), \tag{18}$$

where $\mathbf{m}$ is a vector with components $m_j$, $j = 1, 2, \ldots, N$, such that $m_j$ accounts for the total magnetization of the water in the $j^{\text{th}}$ shell.

While a time-iterative solution of Eq. (18) can be directly obtained according to a scheme such as

$$\mathbf{m}(t + \Delta t) \;\simeq\; \mathbf{m}(t) + \Delta t\ [\mathbf{D} - \mathbf{K}]\ \mathbf{m}(t), \quad \text{or} \tag{19}$$

$$\mathbf{m}(t + \Delta t) \;\simeq\; \mathbf{m}(t) + \frac{\Delta t}{2}\ [\mathbf{D} - \mathbf{K}]\ (\mathbf{m}(t) + \mathbf{m}(t + \Delta t)) \tag{20}$$

($\Delta t$ denotes a short time interval), a much more efficient scheme is the generalized moment expansion (GME) [32, 40]. It has been used here to produce a bi-exponential solution, but a greater number of exponential terms can easily be reproduced by this method in cases where the magnetization would be better described by more than two exponential terms. The method has been thoroughly described elsewhere where it has been applied to Brownian relaxation processes [32], dynamic correlation functions [41], and used to develop the method of continuous microphotolysis [40, 42]. In a forthcoming paper, detailing how the GME can be applied to Eq. (2), the method has also been employed to investigate bi-exponential relaxation in systems of biological capillaries [43].

### 2.3 Outer sphere theory

When $Gd(DTPA)^{2-}$-containing liposomes are placed in an external magnetic field, they produce magnetic field distortions around them. These distortions give rise to outer sphere relaxation: spins outside the liposomes become dephased by heterogeneous Larmor precession frequencies experienced through diffusion. Outer sphere theories of relaxation endeavor to quantitate the degree of relaxation according to the strength and size of the dipoles and the rate of molecular diffusion. The duration (echo time) of the measurement will be seen to play a key role in the application of the established outer sphere theory. The reader may also want to read the thorough discussion presented in [10].

In the presence of magnetic field inhomogeneities, the transverse magnetization quickly decays due to dephasing. If in the sample the range of frequencies is denoted by $\Delta\omega$, and the time it takes for a spin to translate through the whole frequency range is denoted by $\tau$, then when

$$\Delta\omega\,\tau \ll 1, \tag{21}$$

there will be a motional narrowing of the frequency lineshape (spectral density). In other words, the entire range of frequencies is equally experienced by every spin within each precession period (in the rotating frame of the homogeneous field) and the lineshape will be correspondingly narrow. What brings motional narrowing into the present discussion is that motional narrowing decreases (secular) transverse relaxation—for extreme motional narrowing, there will be no spin-spin dephasing since all the spins will precess at the same average frequency.

We first consider free diffusion in a linear magnetic field gradient. Very soon after an initial 90°-pulse the magnetization will decay away due to spin-spin dephasing. There are several ways of rephasing the spins which are all based on the simple Hahn spin echo pulse-sequence [$90° - \tau_H - 180° - \tau_H -$ collect] where $\tau_H$ is the time between pulses. The spin echo, however, does not rephase those spins which have translated through, and thus sampled, variations in the magnetic field during the measurement. For $T_E = 2\tau_H$, the degree to which spins are not rephased, and are therefore relaxed, is given by the Hahn-Torrey expression [33, 34]

$$m(T_E) \sim \exp[-\frac{2}{3}D(\gamma G)^2\tau_H^3] \equiv \exp[-T_E/T_{2H}] \tag{22}$$

where $D$ is the diffusion coefficient and $G$ is a linear magnetic field gradient. In fact, this phenomenon is often called "diffusion weighting" and is used, in a myriad of variations on this simple formulation, to measure the diffusion constant of the spins in a sample [44, 45, 46, 47]. To describe the signal decay from the initial excitation to the time of the echo, one can define a relaxation time $T_{2H}$ which is dependent on the echo time $\tau_H$, as in Eq. (22)

$$T_{2H}^{-1}(T_E) \equiv \frac{1}{3}D(\gamma G)^2\tau_H^2. \tag{23}$$

Since the relaxation rate $T_{2H}^{-1}$ depends on the square of the echo time, it increases rapidly as $\tau_H$ increases. The result, however, applies only to free diffusion in an (unbounded) linear magnetic field gradient. The dependence of the relaxation rate on $\tau_H$ can be explained by the spins sampling an increasingly larger range of frequencies as $\tau_H$ increases. Defining

$$L_H^2 = 2D\tau_H, \tag{24}$$

we can eliminate $D$ from Eq. (23):

$$\frac{1}{T_{2H}}(2\tau_H) = \frac{L_H^2(\gamma G)^2\tau_H^2}{6\tau_H} = (\Delta\omega)^2\tau_H/6. \tag{25}$$

Of course, if there is to be any signal left at time $T_E$, it should hold that $\tau_H < T_{2H}$ since the latter determines how long the signal remains. If $\tau_H \ll T_{2H}$ then Eq. (25) yields $\Delta\omega\tau_H \ll 1$ which implies the well known result that reducing $\tau_H$ reduces the relaxation rate. In fact, the Carr-Purcell sequence of $n$ 180°-pulses, separated by time intervals $2\tau_H/n$, gives rise to a rate diminished by $n^2$ compared to $1/T_{2H}$. Thus, one can view the shortening of the time between 180°-pulses as reducing the available Larmor frequencies, just as spatial boundaries can do [10].

Analogously, if the range of frequencies is restricted, then the $\tau_H^2$ dependence of $1/T_{2H}$ breaks down, and, in fact, $1/T_{2H}$ approaches a constant value. In the system considered here, where $r_2$ (the liposome's outer radius) is the distance of closest approach to the dipole and where $D$ is the diffusion constant of the solvent (water), we define a diffusional correlation time

$$\tau_R = \frac{r_2^2}{D}, \tag{26}$$

which characterizes the time it takes a spin to sample the extremes of the dipole field when it is near the liposome. In this case motional narrowing can occur if translation across the whole variation in frequency space occurs well before, in the rotating frame of the homogenous field, the spins have precessed $1/\Delta\omega$; i. e.,

$$\tau_R \ll 1/\Delta\omega. \tag{27}$$

This motional narrowing, however, will not be observed unless $\tau_H \simeq \tau_R$. The latter is a requirement on the measurement, while Eq. (27) is a requirement on the relationship between the rate of diffusion and the dipole moment.

We will see that as long as $\tau_H < \tau_R$ we can describe the relaxation by Eq. (25), but when Eq. (27) holds and $\tau_H > \tau_R$ then the rate observed will approach a constant value

$$T_{2H} = (\Delta\omega)^2 \tau_R/6, \tag{28}$$

independent of further increases in $\tau_H$. What is interesting is that for very large liposomes, Eq. (27) no longer holds and $T_{2H}$ will continue to increase as long as $\tau_H < T_{2H}$.

So far we have only considered relaxation in the vicinity of the liposomes. A low density of liposomes ($V_f$) has two effects: (i) it reduces the effect of field overlap, and (ii) it introduces a mixing time $\tau_D$ defined by Eq. (5). For low $V_f$ point (i) is quite minor since the field falls off as $r_3^3$. In our simulations we do not consider field overlap. Also for low $V_f$, however, point (ii) can be significant—$\tau_D$ is 100 times greater than $\tau_R$ for $V_f$=0.001. In a log–log plot of $1/T_{2H}$ versus $\tau_H$ one would see that although the line bends over at $\tau_H \simeq \tau_R$, it does not converge to an asymptotic value until $\tau_H > \tau_D$ (see Fig. 7).

**Liposomes as magnetic dipoles**

In the presence of an external magnetic field $B_o$, the difference $\Delta\chi$ between the susceptibility of the Gd(DTPA)$^{2-}$-containing liposomes $\chi_{\mathrm{Gd(DTPA)}}$, and that of the surrounding medium (water) $\chi_{\mathrm{H_2O}}$ induces a dipole field distortion around the liposome. The induced magnetic moment of the liposome is (see, e. g., [48])

$$\mu = \frac{\frac{1+\chi_{\mathrm{Gd(DTPA)}}}{1+\chi_{\mathrm{H_2O}}} - 1}{\frac{1+\chi_{\mathrm{Gd(DTPA)}}}{1+\chi_{\mathrm{H_2O}}} + 2} \, B_o r_1^3 \approx \frac{\Delta\chi}{3} \, B_o r_1^3 \tag{29}$$

where $\Delta\chi = \chi_{\mathrm{Gd(DTPA)}} - \chi_{\mathrm{H_2O}}$ and $r_1$ is the inner radius of the liposome. The precession frequency of the spins is determined by the $z$-component of the dipole field, given by

$$B_z(r,\vartheta) = \mu \, \frac{3\cos^2\vartheta - 1}{r^3} = \Delta\chi B_o (cos^2\vartheta - \frac{1}{3}) \left(\frac{r_1}{r}\right)^3 \tag{30}$$

where $r$ measures the distance from the liposome center.

Values for $\Delta\chi$ are calculated in the Appendix. In Fig. 3 we show how this difference grows non-linearly with the concentration of Gd(DTPA)$^{2-}$. For solutions of 100 mM Gd(DTPA)$^{2-}$, $\Delta\chi \simeq 2.1$ ppm whereas for solutions of 670 mM Gd(DTPA)$^{2-}$, $\Delta\chi \simeq 70$ ppm. This means that susceptibility effects are 30 times greater for a 7-fold increase in Gd(DTPA)$^{2-}$ concentration and, as we will see below, this leads to an almost 1000-fold increase in the outer sphere relaxation!

**Quantum-mechanical approximation**

Outer sphere relaxation theory [10, 25] relates the dephasing or "secular" relaxation rate of the transverse magnetization $T_{2\mathrm{sec}}^{-1}$ in the presence of magnetic dipoles (here, liposomes) to three quantities: (i) to $\delta\omega$, the average magnetic field contribution (in angular frequency units) at the equator of an average magnetized liposome; (ii) to the diffusional correlation time $\tau_R$ defined by Eq. (26); (iii) to the volume fraction occupied by the liposomes

$$V_{\mathrm{f}}' = \left(\frac{r_2}{r_3}\right)^3. \tag{31}$$

This problem has been treated in several works (see e. g., [29, 49]) and the result has presented [10, 25] in the following convenient form,

$$\frac{1}{T_{2\mathrm{sec}}} = \frac{16}{135} V_{\mathrm{f}}'(\delta\omega)^2 \tau_{\mathrm{R}}. \tag{32}$$

As pointed out previously [10], this solution has the same form as Eq. (28), which was derived classically. The discussion surrounding Eq. (28) makes it clear why the validity of Eq. (32) requires that the rapid exchange condition

$$\delta\omega\tau_R \ll 1 \tag{33}$$

be fulfilled. It is also clear that in order to observe this singular rate $1/T_{2\mathrm{sec}}$, the measurement time ($2\tau_H$) should be much longer than the diffusional correlation time ($\tau_R$). When these conditions do not hold, the rate $1/T_{2\mathrm{sec}}$ reverts to $1/T_{2H}$; i. e., it will depend on the square of the echo time $\tau_H$ as long as $\tau_H < T_{2H}$. Values of $\tau_R$ for liposomes with the radii considered above are also shown in Table 1. There we list the product $\delta\omega\tau_R$ only for 670 mM $Gd(DTPA)^{2-}$ liposomes since it is very much less than unity for 100 mM liposomes.

The magnetic field (in angular frequency units) at the equator of a magnetized liposome is nearly given by $\delta\omega = \gamma\Delta\chi B_o/3$ from Eq. (30). The finite thickness of the membrane, however, creates a small modification: since the field at the equator is proportional to the entrapped volume with radius $r_1$, but the distance of closest approach is given by $r_2$, the equatorial field on the liposome outer surface is given by[5]

$$\delta\omega(r_2) = \frac{\gamma\Delta\chi B_o}{3}\left(\frac{r_1}{r_2}\right)^3. \tag{34}$$

Values for $T_{2\mathrm{sec}}^{-1}$ are listed in Table 1. Particularly noteworthy is that $T_{2\mathrm{sec}}^{-1}$ becomes non-negligible only for large liposomes containing a large $Gd(DTPA)^{2-}$ concentration. Indeed there is a nearly 1000-fold increase of $(\delta\omega)^2$ in going from

100 mM to 670 mM $Gd(DTPA)^{2-}$ solution.

TABLE 1

| liposome radius | $\tau_R$ | 100 mM $B_{eq}$ | $(\delta\omega)^2$ | $T_{2sec}^{-1}$ | 670 mM $B_{eq}$ | $(\delta\omega)^2$ | $\delta\omega\tau_R$ | $T_{2sec}^{-1}$ | simulated |
|---|---|---|---|---|---|---|---|---|---|
| 35 | 1.2 | 0.66 | 0.031 | 0.00014 | 18.9 | 25.5 | 0.006 | 0.0175 | |
| 50 | 2.5 | 0.77 | 0.042 | 0.00034 | 21.9 | 34.2 | 0.015 | 0.0415 | 0.108 |
| 100 | 10 | 0.90 | 0.058 | 0.00160 | 25.7 | 47.4 | 0.069 | 0.195 | >0.51 |
| 200 | 40 | 0.97 | 0.068 | 0.00693 | 27.8 | 55.3 | 0.298 | 0.845 | >1.91 |

Estimates for $T_{2sec}^{-1}$ by Eq. (32). Liposome radii [nm] correspond to $r_2$; $\tau_R$ $[10^{-6}\,\mathrm{s}]$ is defined by (26). The equatorial field, $B_{eq}$ $[\mu\mathrm{T}]$, is calculated on the outside of the liposome membrane. The frequency spread, $(\delta\omega)^2$ $[10^6\,\mathrm{s}^{-2}]$, is given by (34). The calculated relaxation rates, $T_{2sec}^{-1}$ [Hz], assume an effective $Gd(DTPA)^{2-}$ concentration of 2 mM, translated by Eq. (3) into a volume fraction of 0.02 for 100 mM liposomes and 0.003 for 670 mM liposomes. Where available, simulation results are provided for comparison (cf. Table 3). For 670 mM $Gd(DTPA)^{2-}$ concentration we also show $\delta\omega\tau_R$.

## 2.4 Simulations

To study the simultaneous occurrence of inner sphere and outer sphere relaxation, we developed a simulation program that models the Bloch-diffusion equations for spin ensembles in simple geometries. Diffusion processes are represented by a random walk of the molecules (see also [50]); spin precession and relaxation are treated classically. The program employed here is described in detail in [51]. Similar Monte-Carlo simulations have been presented in [14, 27, 52, 53, 54]. We know of only one other simulation that endeavored to describe the exchange of particles (corresponding to the inner sphere mechanism) across a barrier (specifically, red blood cell membrane) of specified permeability [27]. In that simulation, however, outer sphere relaxation due to susceptibility differences were not considered. The simulations undertaken here are intended to provide a description of relaxation that incorporates both the inner sphere and outer sphere mechanism. For our purposes here, an accurate description of exchange as a function of permeability is important since we intend to compare the effects of exchange (inner sphere mechanism) with those of susceptibility differences (outer sphere mechanism) in order to determine in how far these mechanisms are additive or collapse into one another, e. g., it is possible that the inner sphere mechanism becomes ineffective since all the spins that reach the liposome interior are already relaxed through the outer sphere mechanism.

The Monte-Carlo simulations produce the magnetization of the sample as the vector sum of all the simulated magnetic spins. As in a Hahn spin echo experiment, the transverse relaxation is measured by the difference between the initial excitation and the echo amplitude after a time $T_E = 2\tau_H$.

The relaxation times in each region, i. e., $T_i$ and $T_0$ for region I and II , respectively, are known. During each time step, $\Delta t$, the spin magnetization is reduced by a factor exp[-$\Delta t/T$], where $T$ is the appropriate relaxation time. We typically simulated measurement times less than 1 ms. Since this time scale is the same as the relaxation time inside the liposome, a simulation of the complete liposome system would be dominated by the small, fast component due to the initial relaxation of the spins inside the liposome. To eliminate this component in favor of the slower bulk relaxation, due to either exchange between regions or outer sphere relaxation, we place all the spins in a nearly uniform distribution outside the liposomes. In Fig. 1 this corresponds to region II, but here the membrane is assumed to be infinitely thin.

Exchange across the (infinitely thin) liposomal membrane is modeled by conditional jumps which occur whenever a particle encounters the membrane. The jump probability is calculated as the ratio of the expected fraction of particles leaving a subvolume [derived from either Eq. (14) or (15)] to the fraction of particles expected to encounter the membrane [calculated by integrating the diffusion equation (2) with $k = 0$ over one time step]. The probabilities found for membranes of permeability $10\,\mu$m/s are 11 and 15 jumps per $10^5$ membrane encounters on the outside and the inside, respectively. These probabilities show only a weak dependence on the liposome size ($\pm 1$ per $10^5$ encounters), and are in good agreement with reports from earlier simulations [27].

Relaxation in the dipole field around the liposome is modeled classically. We consider the magnetization in a frame rotating with the Larmor frequency corresponding to the external field, $\omega_o = \gamma B_o$, and, therefore, spin precession is due to the dipole field only. The magnetization vector assigned to each particle precesses at each time step with a frequency corresponding to the Larmor frequency of the local field felt by the particle averaged over the time step. We do not consider overlap of the field from neighboring liposomes as has been done in [55]. As long as the distance between liposomes is several times larger than their radius and the dipole moment is not too large then this effect is negligible. If, for example, $5\,r_2 \simeq r_3$ corresponding to $V_f = 0.01$, then the field felt at one liposome from a nearest neighbor is on the order of $B_{\rm eq}(r_2/2r_3)^3 \simeq 0.001\,B_{\rm eq}$ where $B_{\rm eq}$ is the field at the equator as given by Eq. (30).

The finite volume fraction $V_f$ is accounted for by a reflective outer boundary at radius $r_3$ as in Figs. 1 and 2. At a reflective boundary the effect of diffusional edge enhancement in the presence of magnetic field gradients induces a slight enhancement in the magnetization [56]; this effect should be rather negligible for the small gradients considered here.

In our simulations we used $\Delta\chi[670\,mM] = 60 \times 10^{-6}$ and a $1.5\,\mathrm{T}$ magnetic field as employed in [36]. The resulting dipole moment for a 400 nm outer diameter liposome is then $\mu(400\,\mathrm{nm}) = 2.22 \times 10^{-25}\,\mathrm{Tm}^3$.

**Simulation tests** In order to make certain that our simulation program accurately describes the complex interactions of diffusion, exchange, and spin precession in inhomogeneous fields, we performed a series of tests. To check our simulation program accurately describes relaxation in a magnetic field gradient, we simulated a Hahn spin-echo experiment with different linear field gradients. The observed relaxation rate was in excellent agreement with the Hahn-Torrey relaxation (22), with a deviation of less than $0.5\,\%$ at time $t = 2\tau$. Spin precession in a dipole field was also tested by turning off the Brownian motions of the particles and monitoring their precession at various positions in the dipole field. The precession frequency observed, $\omega_{\text{obs}}(\mathbf{r})$, was compared with the frequency calculated from the parameters used, $\omega_{\text{dip}}(\mathbf{r}) = \gamma B_z(\mathbf{r})$, where $B_z$ is given in Eq. (30) and where $\gamma$ is the gyromagnetic ratio. The difference was found to be less than 0.01 %.

The question of what step size accurately describes the combined processes of diffusion and exchange has also been investigated. In general, shorter time steps will more closely reflect the microscopic processes and, therefore, give more precise results, yet the time steps need be chosen as long as possible to minimize simulation time. We simulated diffusion in the absence of field inhomogeneities in order to monitor the success of a Monte Carlo description of the inner sphere mechanism and to compare the results with that for the two-site model above. In the absence of a dipole field we chose time steps such that particles on average do not travel more than the radius of the smallest region during one time step; time steps of $10^{-7}$ s satisfied this consideration. In the presence of magnetic field inhomogeneities smaller time steps can be necessary. Simulations were run for liposomes with 400 nm outer diameter containing 670 mM $\text{Gd(DTPA)}^{2-}$. The dipole moment of the liposome in an external field of 1.5 T is then $2.22\times10^{-25}\,\text{Tm}^3$. Running simulations with a constant echo time ($2\tau$) but different time steps shows that the relaxation rate increases as the time step is increased. This is attributed to insufficient sampling of the dipole field for long time steps. Thus, time steps of $10^{-7}$ s were chosen to compromise between achieved accuracy and feasibility of simulations (cf. Table 2). Over this time step water molecules diffuse approximately 14 nm. We therefore employed simulations of outer sphere relaxation only to liposomes of at least 100 nm diameter. What is also interesting is that if the time steps are taken too large especially for the smaller liposomes, the sampling becomes random, resulting in a relatively higher relaxation rate for short measurement times, i. e., times where a single spin can not sample the whole frequency range. This has been demonstrated nicely in [53]. We thus expect the results to be more accurate for larger liposomes.

The simulations were carried out on a Connection Machine CM-200, a massively parallel machine (32,678 processors) that allowed us to complete these computationally intensive simulations. The large number of processors was utilized by assigning

TABLE 2

| echo time $2\tau$ | time step | outer sphere relaxation rate |
| --- | --- | --- |
| $12\,\mu$s | $10^{-6}$ s | $0.0941\,s^{-1}$ |
| | $10^{-7}$ s | $0.0865\,s^{-1}$ |
| | $10^{-8}$ s | $0.0862\,s^{-1}$ |

Effect of the choice of the simulation time steps on the observed outer sphere relaxation rate for 400 nm liposomes. There is rather good agreement for time steps of $10^{-7}$ and $10^{-8}$ s, the difference being only 0.3 %, compared to a difference of almost 10 % between $10^{-7}$ and $10^{-6}$ s. For longer time steps, however, the rates differ significantly, indicating that using time steps larger than $10^{-7}$ s will almost certainly yield unreliable results. For smaller liposomes even shorter time steps may be necessary (see Fig. 7).

one spin to each processor, or, more precisely, one spin per virtual processor when the number of spins exceeds the number of available processors. Since the CM-200 is a SIMD (single instruction, multiple data) machine, each instruction in a program is simultaneously executed on all the processors, and, therefore, all the spin trajectories are independently calculated in parallel. Only at times when the overall magnetization is recorded, is inter-processor communication necessary in order to sum up the individual magnetization of all the processors.

The computational requirements were (1) to have a sufficient number of spins to yield statistically meaningful results, and (2) to use time steps short enough to adequately sample the features of the diffusion space, especially the dipole field around the liposomes. Related to the small size of liposomes, this latter requirement makes our simulations computationally more intensive than similar simulations carried out for larger systems [14] and allows only relatively short times to be simulated.

For simulations of outer sphere relaxation 65,536 spins gave well-converged relaxation rates. In simulations of inner sphere relaxation, we used 262,144 spins to reduce statistical fluctuations that seem to be unavoidable by our model of exchange across the liposome membrane. Typical simulations required between 30 minutes and 4 hours, depending on the number of particles and the simulated echo time.

# 3 Results and Discussion

A major criterion for the evaluation of a contrast agent is its ability to increase the bulk relaxation rate of the tissue into which it is introduced. As the mechanisms described above are applied to real systems, a key question will be what relaxivity do liposomal contrast agents actually provide, i. e., how well do they work?

## 3.1 Inner Sphere (Exchange) Models of Relaxation

### Two-site model

Here we apply the two-site model described above to data published in [36]. In Fig. 4 we plot the permeability (determined via Eq. 16) as a function of mean outer diameter for egg PC/cholesterol = 6/4 liposomes with internal relaxation rates of $1/T_i = 1869\,\mathrm{Hz}$, at a volume fraction $V_f = 0.003$ (values from [36]). We observe that while no single $P_d$ value can match all the liposome sizes, a value of $16\,\mu\mathrm{m/s}$ is in fairly good agreement. Previously [26], we applied a simple one-site model to the same data [36] where we assumed that because the inside relaxation rate is high (on the order of 2000 Hz), the magnetization of spins exchanging into the liposomes should vanish before they exit. This approach yielded a value of $P_d = 9.4\,\mu\mathrm{m/s}$—not too different from $16\,\mu\mathrm{m/s}$ as has been derived here. That the value is nearly double in the two-site model is due to the exchange time $\tau_{\mathrm{io}}$ being comparable to the inside relaxation time $T_i$.

As mentioned above, in the context of liposomes as MRI contrast agents, the crucial issue is the degree of relaxation rate enhancement. In Fig. 5 we present the relaxation rate enhancement ($1/T_{\mathrm{para}}$) as a function of liposome size for the relaxivity $1/T_i = 1869\,\mathrm{Hz}$, volume fraction $V_f = 0.003$ (as above), and the derived permeability of $16\,\mu\mathrm{m/s}$. We present $1/T_{\mathrm{para}}$ also for a lower relaxivity $1/T_i = 421\,\mathrm{Hz}$ (interpolated from [25]) and permeability $8.7\,\mu\mathrm{m/s}$ reported in [25] for similarly constructed liposomes (POPC/cholesterol = 6/4) at 25°C. Since no temperature was reported for the earlier data we chose this temperature for comparative purposes.

**Relaxivity dependence on liposomal size** As one can see from Fig. 5, the dependence of the relaxation rate enhancement $T_{\text{para}}^{-1}$ on the liposome radius for liposomes filled with a moderate amount of $\text{Gd(DTPA)}^{2-}$ (100 mM) is weaker than for liposomes filled with significantly more contrast agent (670 mM) in which case the size dependence is strongly non-linear. Also shown is that the dependence on size is further reduced by an increase in $P_d$, a point made clear by inspection of Eq. 17.

By modern preparation techniques, involving the extrusion of liposomes through polycarbonate filters, one may achieve a distribution of $\pm 20$ nm in liposome diameter [57]. We have found that a symmetric variance in the size distribution of liposomes has very little effect on the system relaxation rate enhancement $T_{\text{para}}^{-1}$. In Fig. 6 we compare $T_{\text{para}}^{-1}$ for exact liposome diameters with $T_{\text{para}}^{-1}$ for distributions of liposome diameters, each with a variance of 20 nm, and find only a few percent change. Even for normal distributions with standard deviation of 40 nm one does not see significant deviations. On the other hand, if the *mean* diameter of the distribution is significantly uncertain, there will be a correspondingly large uncertainty in the rate enhancement one could expect. In Fig. 6 we demonstrate this by plotting $T_{\text{para}}^{-1}$ as a function of extrusion filter pore size, assuming that the mean diameter of the liposomes is 70 % of the pore diameter. This corresponds to a mean liposome diameter of 70 nm being produced by a 100 nm filter, a particular case realized in a histogram of diameters observed by cryo-transmission electron microscopy for DPPC liposomes prepared by ten passes through a 100 nm polycarbonate filter (see [57], p. 280). Interestingly, this is essentially the same distribution reported in [36] for egg PC/cholesterol = 6/4 liposomes passed ten times through a 50 nm polycarbonate filter! Thus, the composition of the membranes seems to greatly affect the outcome of the extrusion technique.

**Relaxivity dependence on $\text{Gd(DTPA)}^{2-}$ concentration** In Eq. 17 one can observe that the smaller and the more permeable the liposomes, the more effective an increase in $1/T_i$ (i. e., an increased concentration of entrapped contrast agent) will be in increasing the bulk rate. Since $T_{\mathrm{para}}^{-1}$ is proportional to the inverse of the sum of two quantities, $(\tau_{io} + T_i)$, its maximum occurs when they are roughly equal. Increasing the permeability without increasing the concentration of entrapped contrast agent will not increase the rate enhancement indefinitely, but will instead make the rate enhancement insensitive to liposome size. As $\tau_{io}$ is made vanishingly small, the bulk rate will become just the volume-weighted average of the entrapped contrast agent rate with the native rate. For purposes of reproducibility in relaxation rate enhancement, it may be seen as an advantage that the size dependence of relaxivity goes down with higher membrane permeabilities (cf. Fig. 5).

**Permeability measurements** To evaluate the effects of taking into account the membrane thickness and water displaced by the contrast agent, we apply both Eqs. (13) and (16) to observations of cholesterol-free POPC liposomes with an outer diameter of 50 nm [25]. For these (rather small) liposomes, Eq. (16) yields the permeability values of 10 $\mu$m/s and 28 $\mu$m/s at 5°C and 35°C, respectively, a reduction in the membrane permeability of 20 % compared to what is obtained by Eq. (13). This, however, brings the values only slightly closer into agreement with a permeability measurement of $P_d$=6.4 $\mu$m/s for 300 nm liposomes by $D_2O$ transport at 23°C [58], a value about 1/6 the results in [25]. On the other hand, when one further corrects for water displacement by reducing $V_f$ by 20% (corresponding to 100 mM—see Appendix), one finds that $P_d$ nearly doubles.

### Discrete shell and random walk models

We have employed the generalized moment expansion (GME) through a finite difference approximation (as outlined above). The liposomes present a particularly simple application because they are spherically symmetric. For all the permeablities considered in the scope of this work ($P_d \leq$1–500 $\mu$m/s), this algorithm produces the same relaxation rates as the two-site model.

Random walk simulations of inner sphere relaxation agree only qualitatively with the results from the two models above. The quantitative disagreement between the relaxation rates given by the two site model and those produced by simulation, suggests an inaccuracy in the calculation of a membrane transmission probability as a function of permeability (cf. Table 4).

### 3.2 Outer Sphere Relaxation—$T_2$ only

Using a liposome diameter of 100 nm, an internal $Gd(DTPA)^{2-}$ concentration of 100 mM, an effective concentration of 1 mM, and an external field of 1 T we find by Eq. (32)

$$\frac{1}{T_{2\text{sec}}} \simeq 87 \times 10^{-6}\,\text{Hz}, \tag{35}$$

approximately a factor 20 larger than the value estimated in [28] for the same situation. For larger liposomes the equatorial field increases slightly, but $\tau_R$ increases with the square of the (inner) radius. For liposomes of 400 nm diameter this implies an increase by a factor of about 16 compared to the value above. We found (see Fig. 3) that for higher $Gd(DTPA)^{2-}$ concentrations inside the liposomes, the susceptibility difference between inside and outside the liposomes increases nonlinearly. The square of this increase enters Eq. (32) via $(\delta\omega)^2$, and, therefore, large liposomes containing a more concentrated $Gd(DTPA)^{2-}$ solution show relaxation rates on the order of 1 Hz. This is probably too small for imaging applications.

Incidently, this coincides with estimates of outer sphere relaxation in striated muscle tissue done by Packer [31] based on results by Robertson [30]. The frequency spread between highest and lowest frequency induced in the muscle tissue $\Delta\omega$ has been reported as being on the order of $1.4{\times}10^3\,\text{s}^{-1}$ [59], from which Packer finds a relaxation rate of 0.5 Hz. He thus concludes that in muscle tissue relaxation effects due outer sphere relaxation are negligible (approx. 0.2 % for echo times of 5 ms).

Thus, for "normal" size liposomes, outer sphere relaxation appears to be insignificant for contrast enhancement. Nevertheless, very large, multivesicular liposomes containing $Gd(DTPA)^{2-}$ have also been employed to improve contrast in MRI. In one such effort [60] multivesicular liposomes on the order of 10 $\mu$m in diameter were prepared with an internal $Gd(DTPA)^{2-}$ concentration of 33 mM. This corresponds to $\Delta\chi = 0.37$ ppm. In this case the equatorial presession frequency $\delta\omega$ at in an external field of $B_o = 2\,\mathrm{T}$ would be

$$\delta\omega = 2\pi\,\gamma\,\Delta\chi\,B_o/3 \simeq 66\mathrm{s}^{-1} \tag{36}$$

The product $\delta\omega\tau_R \simeq 0.8$ which means the validity of $1/T_{2\mathrm{sec}}$ (32) is unlikely.

If we consider a $T_E = 2\tau_H = 20\,\mathrm{ms}$ experiment, then since $\tau_R \simeq 12\,\mathrm{ms}$ we can use the Hahn-Torrey result. In fact the water spins will not move more than about $9\,\mu\mathrm{m}$, which, incidently, is about twice the liposome radius $r_2$ under consideration. If we assume that about half the spins a distance $r_2$ away come very close to the liposome in the time $T_E$, then we can estimate the relaxation rate for these spins by the Hahn-Torrey relation (22) where

$$G \simeq \frac{B(r = r_2) - B(r = 2r_2)}{r_2} = \frac{\Delta\chi\,B_o(1 - 1/8)}{3r_2} = \frac{7}{24}\frac{\Delta\chi\,B_o}{r_2} \tag{37}$$

Using Eq. (23) we find a rate for those spins in the vicinty of the liposomes, $1/T_{2H} \simeq 0.2\,\mathrm{Hz}$, which is quite small.

If however, the concentration of $\mathrm{Gd(DTPA)}^{2-}$ were much higher—say on the order of 600 mM—then the picture would change dramatically. In this case $\Delta\chi = 60\,\mathrm{ppm}$, and, therefore, $\delta\omega = 1.07 \times 10^4\,\mathrm{s}^{-1}$ for the otherwise same conditions in Eq. (36). Now the product $\delta\omega\tau_R \simeq 133$, well out of the realm of validity for $1/T_{2\mathrm{sec}}$. By Eq. (37) $G \simeq 7 \times 10^4\,\mathrm{G/cm}$, and $1/T_{2H} \simeq 4700\,\mathrm{Hz}$! Although this rate is even higher than what is even possible in a *solution* of contrast agent (in [36] it is about 2000 Hz for 670 mM $\mathrm{Gd(DTPA)}^{2-}$), it must be kept in mind that this rate is only for those spins rather close to the liposomes—the decay will be highly heterogeneous, i. e., multiexponential. This problem has recently been investigated in [43], where the generalized moment expansion has been used. An analogous problem involving superparamagnetic contrast agents taken up by the Kupffer cells of the liver has been treated semi-analytically in [9].

**Simulation results** Comparing the results of our simulations to the predictions from the outer sphere relaxation model, we find that our simulations generally yield slightly higher relaxation rates, as shown in Table 3.

TABLE 3

| | relaxation rate | | | ratio | |
|---|---|---|---|---|---|
| diameter [nm] | simulation | (extrapol.) | theory | | |
| 100 | 0.108 | | 0.0415 | 2.6 | |
| 200 | >0.51 | (0.52) | 0.195 | 2.6 | (2.6) |
| 400 | >1.91 | (2.24) | 0.845 | 2.2 | (2.6) |

Outer sphere relaxation rates [Hz] determined from simulations and calculated from Eq. (32). All values are calculated for liposomes containing 670 mM Gd(DTPA)$^{2-}$ for a volume fraction of 0.003. The outer sphere relaxation rate for 100 nm liposomes has already reached its asymptotic value (see Fig. 7) after 0.4 ms. For the largest echo times accessible to simulations, 1.6 ms, the asymptotic rate is not quite achieved for a 200 nm diameter and will probably increase by a factor of 1.2 for a 400 nm diameter. By extrapolation (see Eq. (38)), we estimate the asymptotic rates for these two diameters (shown in parentheses) and see that the ratio will then be approximately 2.6.

The computer simulations have yielded the outer sphere relaxation rates for liposomes of different sizes at different echo times. The results are shown in Fig. 7 As discussed above we expect each curve to show three distinct regimes, (1) a short-time regime $\tau_H < \tau_R$ where the relaxation rate depends on $\tau_H^2$, (2) a transition regime $\tau_R < \tau_H < \tau_D$, and (3) a long-time regime $\tau_H > \tau_D$ where the relaxation rate converges asymptotically. At a fixed volume fraction of 0.003, for liposomes with outer diameters of 100, 200, and 400 nm, the times $\tau_R$ are 0.0025, 0.01, and 0.04 ms, respectively, while the times $\tau_D$ are 0.042, 0.19 and 0.79 ms, respectively. In Fig. 7 it appears that the curves agree well with these estimates of the transition times.

Using Eq. (32) together with Eqs. (26), (31), and (34), we can write the dependence on the liposome radius more explicitly

$$T_{2\text{sec}}^{-1}(r_2) = \frac{16}{135}\frac{C_{\text{eff}}}{C_o}\left(2\pi\gamma\frac{\Delta\chi}{3}B_o\right)^2 \frac{1}{D}\,\frac{(r_2-d)^3}{r_2}, \tag{38}$$

where $d$ is the membrane thickness.

We estimate the asymptotic relaxation rates for 200 nm and 400 nm liposomes using the $r_2$-dependence from Eq. (38) and the asymptotic rate for 100 nm liposomes from Fig. 7 to find 0.52 Hz and 2.24 Hz, respectively. These rates agree with extrapolations of the simulation data shown in Fig. 7. The simulated relaxation rates are then 2.6 times higher than the corresponding outer sphere predictions.

For short echo times ($\tau_H < \tau_R$), large liposomes exhibit slower relaxation rates than small liposomes, reflecting the fact that for smaller liposomes the individual spins get dephased more quickly.

### 3.3 Combined Mechanisms of Relaxation

In a laboratory experiment inner and outer sphere relaxation mechanisms act in parallel and cannot usually be distinguished.[6] Simulations, however, allow us to differentiate the two effects by turning them on and off separately. Nonetheless, all our simulations indicate that the rates due to the two processes simply add up as shown in Table 4.

That the rates add algebraically is indicative of a parallel process, as opposed to a sequential one. That the *times* $\tau_{\mathrm{io}}$ and $T_i$ are being added in the formula for $1/T_{\mathrm{para}}$ is a consequence of the processes being sequential: spins have to first reach the inside of the liposome and then get relaxed. On the other hand, the inner and outer sphere relaxation mechanisms act in parallel since spins can always relax through either process and do not have to wait for one to finish before beginning the other.

## 4 Conclusions

The relaxation mechanisms of paramagnetic liposomal contrast agents (ensomes) in MRI have been described here in detail and are well understood. This knowledge, indispensible for the innovation and refinement of liposomal agents, also creates important inroads in the consideration of liposomes as a model of tissue cells and capillaries, and for the characterization water transport and diffusion. Membrane

TABLE 4

| r [nm] | inner sphere | | outer sphere | | combined | |
|---|---|---|---|---|---|---|
| | two-site | simulation | theory | simulation | analytic sum | simulation |
| 50 | 1.52 | 0.545 | 0.0415 | 0.108 | 1.64 | 0.65 |
| 100 | 0.80 | 0.196 | 0.168 | 0.51 | 0.97 | 0.71 |
| 200 | 0.40 | 0.080 | 0.845 | 1.91 | 1.25 | 1.99 |
| 500 | 0.17 | | 5.38 | | 5.55 | |

Bulk relaxation rates [$s^{-1}$] as a function of liposome radii $r$ for the inner sphere and outer sphere relaxation mechanisms. The internal $Gd(DTPA)^{2-}$ concentration is 670 mM, resulting in an internal relaxation time of 0.5 ms [36], the effective concentration is 2.0 mM, and the external field is 1.5 T. A membrane permeability of $9.4\times10^{-4}$ cm/s and a water diffusion constant of $10^{-5}$ cm$^2$/s has been assumed.

permeabilities, for example, can be measured by the employment of the inner sphere mechanism with attention paid to the limitations detailed above.

Liposomal contrast agents have already been reported to improve image contrast in many animal studies. For example, Unger et al. have reported significantly improved contrast between liver and tumor, and have reported that smaller liposomes cause greater enhancement [19]. In having a mechanistic understanding of contrast agents, one can see their essential limitations as well as how to improve them, especially where there are physical constraints of temperature, toxicity, tissue absorbance, and so on.

Where very novel techniques are being tried, such as the use of giant liposomes, it is critical to consider all possible mechanisms available. In a recent study, for example, giant liposomes ($\sim 10\,\mu$m diameter) have been used to deliver the $Gd(DTPA)^{2-}$ contrast agent to rabbit brain [60]. Such liposomes, however, are not just leaky bags of contrast agent—they are potentially very powerful outer sphere contrast agents as shown above. In fact, because of their multivesicular nature and their very small surface to volume ratio, they would make rather poor inner sphere relaxation agents. Yet as outer sphere relaxation agents their tissue specificity and agent retention capacity may make them better suited for enhancing capillary beds than other techniques. Observing that such liposomal agents may be exploited as outer sphere agents also suggests $T_2$-weighting for imaging instead of the $T_1$-weighting reported in [60].

Nonetheless, for the smaller, unilamellar vesicles, inner sphere relaxation will dominate the relaxation enhancement of the bulk, giving rise to typically much more than 90% of the enhancement. This enhancement $1/T_{\text{para}}$, is given by Eq. 17 which can be summarized as

$$1/T_{\text{para}} = \text{bulk rate} = \frac{\text{number of liposomes}}{\frac{\text{size}}{\text{permeability}} + \text{agent relax. time}} = \frac{\text{conc.}}{\tau_{\text{io}} + T_i} \tag{39}$$

Since $T_{\text{para}}$ is proportional to the sum of two terms, $\tau_{io} + T_i$, it is especially advantageous to keep both small for highest bulk rate enhancement $1/T_{\text{para}}$. One also sees that if the permeability is rather low ($\sim 10\,\mu\text{m/s}$), then $1/T_{\text{para}}$ depends greatly on liposome size, especially for high concentrations of entrapped contrast agent. We have also observed, however, that for a Gaussian (normal) distribution of liposome diameters, a wide variance (even $\pm 40\,\text{nm}$) hardly affects the relaxation rate of the bulk.

It is perhaps worth reiterating that smaller, more permeable liposomes may only very marginally increase the bulk relaxation rate. Since at physiological temperatures, $P_d \simeq 50 \times 10^{-4}\,\text{cm/s}$, $\tau_{\text{io}}$ is about 0.3 ms for 100 nm diameter liposomes. For a $\text{Gd(DTPA)}^{2-}$ concentration of 100 mM, as employed in [25], the inside relaxation time $T_i$ is about 2.7 ms. This means that the inside rate is limiting the relaxation enhancement, and increasing the permeability and decreasing the radius, both by a factor of 2, will lower $\tau_{\text{io}}$ to 0.08 ms, but will change the quantity $\frac{1}{\tau_{\text{io}}+T_i}$ by less than 10%. On the other hand, doubling just the concentration of $\text{Gd(DTPA)}^{2-}$ will nearly double $\frac{1}{\tau_{\text{io}}+T_i}$.

The simulations have yielded higher values for the outer sphere relaxation than what the theory predicts. In all the results (see Table 3) we find about 2.6 times the relaxation predicted by the quantum mechanical outer sphere theory. On the other hand, the plots of the relaxation as a function of time behave in accordance with our expectations. What is more, we find that the deviation from outer sphere relaxation theory appears to be a constant factor. There is no obvious explanation for the discrepancy.

Nevertheless, independent of numerical comparisons between simulation results and analytic results, there is no evidence that the inner sphere and outer sphere mechanisms do not act independently—the mechanisms of relaxation are additive, and typically the outer sphere relaxation is a minor effect.

## 5 Acknowledgments

We would like to thank David White of the Dept. of Radiology at UCSF for helpful comments on magnetic susceptibility, Christian Kurrer at UIUC for fruitful discussions, and Richard Magin, Andrew Webb, and Lisa Wilmes at UIUC for useful comments on liposomes. We also thank Walter Hirth of Mallinckrodt Medical, St. Louis, MO for kindly measuring the water displaced by $Gd(DTPA)^{2-}$. This work has been completed at the Resource for Concurrent Biological Computing at the University of Illinois with the funding of the National Institutes of Health (grant P41RR05969). Computer time on a Thinking Machines CM-200 has been made available through the National Center for Supercomputing Applications funded by the National Science Foundation (grant DMB920007N). D. B. is supported by an NIH training grant.

## Appendix

**Susceptibility values** Here we calculate $\Delta\chi = \chi_{\mathrm{Gd(DTPA)}} - \chi_{\mathrm{H_2O}}$ which appears in Eqs. (29) and (30) We begin with the molar susceptibility for $Gd(DTPA)^{2-}$ in the cgs system of units $\chi^{\mathrm{cgs}}_{\mathrm{Gd(DTPA)}} = 2.55 \times 10^{-2}$ [61, 62]. While the susceptibility $\chi$ is dimensionless, the magnetostatic equations change with the system of units used. To convert from cgs to SI, $\chi^{\mathrm{cgs}}$ has to be multiplied by $4\pi$. To convert these susceptibilities to the ones used in Eq. (29) we use

$$\chi^{\mathrm{SI}} = 4\pi\,\chi^{\mathrm{cgs}}_{\mathrm{molar}}\frac{\rho}{A} = 4\pi\,\chi^{\mathrm{cgs}}_{\mathrm{molar}}\left(\frac{\#\text{ of moles}}{\mathrm{cm}^3}\right), \tag{40}$$

where $\rho$ is the mass density and $A$ the molecular weight of the substance of interest. Thus, in SI units $\chi^{\mathrm{cgs}}_{\mathrm{Gd(DTPA)}}$ becomes

$$\chi^{\mathrm{SI}}_{\mathrm{Gd(DTPA)}} = 320 \times 10^{-6} C_o, \tag{41}$$

where $C_o$ is the molar concentration of the $\mathrm{Gd(DTPA)}^{2-}$ solution. Due to the high susceptibility value of Gd, we can ignore the susceptibility contribution of cations, which, in case of $\mathrm{Na_2Gd(DTPA)}$, is three orders of magnitude less than the Gd contribution.

In order to calculate the susceptibility for a solution of $\mathrm{Gd(DTPA)}^{2-}$, we add the susceptibilities of $\mathrm{Gd(DTPA)}^{2-}$ and water, weighted by the relative mass fractions according to

$$\chi_{\mathrm{weighted}} = m'_{\mathrm{Gd(DTPA)}}\,\chi^{\mathrm{SI}}_{\mathrm{Gd(DTPA)}} + (1 - m'_{\mathrm{Gd(DTPA)}})\,\chi^{\mathrm{SI}}_{\mathrm{H_2O}}, \tag{42}$$

where $m'_{\mathrm{Gd(DTPA)}} = \frac{m_{\mathrm{Gd(DTPA)}}}{m_{\mathrm{Gd(DTPA)}} + m_{\mathrm{H_2O}}}$ is the relative mass fraction of $\mathrm{Gd(DTPA)}^{2-}$ in the solution and $\chi^{\mathrm{SI}}_{\mathrm{H_2O}} = -1.6 \times 10^{-7}\,C_{\mathrm{H_2O}}$, calculated for the molar concentration of the remaining water using Eq. (41) and $\chi^{\mathrm{cgs}}_{\mathrm{H_2O}} = -12.97 \times 10^{-6}$ [63].

Finally, since the molarity rather than the molality of the solutions is quoted in the literature, we must know how many moles of water are displaced by each mole of $\mathrm{Gd(DTPA)}^{2-}$. Recent measurements [38] indicate displacements of 170 mL and 257 mL per mole $\mathrm{Gd(DTPA)}^{2-}$ for $\mathrm{Gd(DTPA)}^{2-}$ concentrations of 100 and 700 mM, respectively. This offsets the value of $\Delta\chi = \chi_{\mathrm{weighted}} - \chi^{\mathrm{SI}}_{\mathrm{H_2O}}$ only slightly. In Fig. 3 we plot $\chi^{\mathrm{SI}}_{\mathrm{molar}}$ versus $\mathrm{Gd(DTPA)}^{2-}$ concentration, assuming that 257 mL water is displaced per mole of $\mathrm{Gd(DTPA)}^{2-}$, and indicate the dependence on the water displacement by including a curve where no water has been displaced by the $\mathrm{Gd(DTPA)}^{2-}$.

# References


[1] Conlon, T. and Outhred, R. 1972. Water Diffusion Permeability of Erythrocytes Using an NMR Technique. Biochim. Biophys. Acta, 288:354.

[2] Haran, N. and Shporer, M. 1976. Study of Water Permeability through Phospholipid Vesicle Membranes by $^{17}$O-NMR. Biochim. Biophys. Acta, 462:638.

[3] Magin, R. L., Niesman, M. R., and Bačić, G. 1990. The Influence of Fluidity on Membrane Permeability: Correspondence Between Studies of Membrane Models and Simple Biological Systems. In Aloia, R. C., Curtain, C. C., and Gorden, L. M. (Eds.), Advances in Membrane Fluidity, Band 4. A. R. Liss, New York.

[4] Schwendener, R. A., Wüthrich, R., Duewell, S., Westera, G., and von Schulthess, G. K. 1989. Small unilaminar liposomes as MR contrast agents loaded with paramagnetic Mn-, Gd- and Fe-DTPA-stearate complexes. International Journal of Pharmaceutics, 49:249.

[5] Tilcock, C., Ahkong, Q. F., Koenig, S. H., Brown, III, R. D., Davis, M., and Kabalka, G. 1992. The Design of Liposomal Paramagnetic MR Agents: Effect of Vesicle Size upon the Relaxivity of Surface-Incorporated Lipophillic Chelates. Magn. Reson. in Med., 27:44.

[6] Brasch, R. C., Weinmann, H.-J., and Wesbey, G. E. 1984. Contrast-Enhanced NMR Imaging: Animal Studies Using Gd-DTPA Complex. Am. J. Roentgenol., 142:625.

[7] Gregoriadis, G. (Ed.) 1993. Liposome Technology, Volume 2. CRC Press, Boca Raton, Florida, 2 edition.

[8] Knight, C. G. (Ed.) 1981. Liposomes: From Physical Structure to Therapeutic Applications. Elsevier, North-Holland, Amsterdam.

[9] Bauer, W. R. and Schulten, K. 1992. Theory of Contrast Agents in Magnetic Resonance Imaging: Coupling of Spin Relaxation and Transport. Magn. Reson. in Med., 26:16.

[10] Gillis, P. and Koenig, S. H. 1987. Transverse Relaxation of Solvent Protons Induced by Magnetized Spheres: Application to Ferritin, Erythocytes, and Magnetite. Magn. Reson. in Med., 5:323.

[11] Thulborn, K. R., Waterton, J. C., Matthews, P. M., and Radda, G. K. 1982. Oxygenation Dependence of the Transverse Relaxation Time of Water Protons in Whole Blood at High Field. Biochimica et Biophysica Acta, 714:265.

[12] Pirkle, J. L., Ashley, D. L., and Goldstein, J. H. 1979. Pulse Nuclear Magnetic Resonance Measurements of Water Exchange Across the Erythrocyte Membrane Employing a Low Mn Concentration. Biophys. J., 25:389.

[13] Morariu, V. V. and Benga, G. 1977. Evaluation of a Nuclear Magnetic Resonance Technique for the Study of Water Exchange Through Erythrocyte Membranes in Normal and Pathological Subjects. Biochim. Biophys. Acta, 469:301.

[14] Fisel, C. R., Ackerman, J. L., Buxton, R. B., Garrido, L., Belliveau, J. W., Rosen, B. R., and Brady, T. J. 1991. MR Contrast Due to Microscopically Heterogeneous Magnetic Susceptibility: Numerical Simulations and Applications to Cerebral Physiology. Magn. Reson. in Med., 17:336.

[15] Weinmann, H.-J., Brasch, R. C., Press, W.-R., and Wesbey, G. E. 1984. Characteristics of Gd-DTPA Complex: A Potential NMR Contrast Agent. Am. J. Roentgenol., 142:619.

[16] Gadian, D. G., Payne, J. A., Bryant, D. J., Young, I. R., Carr, D. H., and Bydder, G. M. 1985. Gadolinium-DTPA as a Contrast Agent in MR Imaging—Theoretical Projectioins and Practical Observations. J. Computer Assisted Tomography, 9:242.

[17] Bačić, G., Niesman, M. R., Magin, R. L., and Swartz, H. M. 1989. NMR and ESR Study of Liposome Delivery of $Mn^{2+}$ to Murine Liver. Magn. Reson. in Med., 13:44.

[18] Kabalka, G., Buonocore, E., Hubner, K., Moss, T., Norley, N., and Huang, L. 1987. Gadolinium-labelled Liposomes, targeted MR contrast agents for the liver and the spleen. Radiology, 163:255.

[19] Unger, E. C., Winokur, T., MacDougall, P., Rosenblum, J., Clair, M., Gatenby, R., and Tilcock, C. 1989. Hepatic Metastases: Liposomal Gd-DTPA-enhanced MR Imaging. Radiology, 171:81.

[20] Gregoriadis, G. and Florence, A. T. 1993. Liposomes in Drug Delivery—Clinical, Diagnostic and Ophthalmic Potential. Drugs, 45:15.

[21] Koenig, S. H., Brown, III, R. D., Kurland, R., and Ohki, S. 1988. Relaxivity and Binding of $Mn^{2+}$ Ions in Solutions of Phosphatidylserine Vesicles. Magn. Reson. in Med., 7:133.

[22] Bloembergen, N. 1957. J. Chem. Phys., 27:672.

[23] Brownstein, K. R. and Tarr, C. E. 1979. Importance of Classical Diffusion in NMR Studies of Water in Biological Cells. Physical Review A, 19:2446.

[24] Barsky, D., Pütz, B., Schulten, K., J. C. Alameda, J., and Magin, R. L. Theoretical Description of Liposome-Entrapped MR Contrast Agents: Influence of Size and Membrane Permeability, In "Eighth Annual Scientific Meeting and Exhibition, Works in Progress". Society of Magnetic Resonance in Medicine, Inc., 1989.

[25] Koenig, S. H., Ahkong, Q. F., Brown, III, R. D., Lafleur, M., Spiller, M., Unger, E., and Tilcock, C. 1992. Permeability of Liposomal Membranes to Water—Results from the Magnetic Field Dependence of $T_1$ of Solvent Protons in Suspensions of Vesicles with Entrapped Paramagnetic Ions. Magn. Reson. in Med., 23:275.

[26] Barsky, D., Pütz, B., Schulten, K., and Magin, R. L. 1992. Theory of Paramagnetic Contrast Agents in Liposome Systems. Magn. Reson. in Med., 24:1.

[27] Santyr, G. E., Kay, I., Henkelman, R. M., and Bronskill, M. J. 1990. Diffusive Exchange Anaylsis of Two-Component $T_2$ Relaxation of Red Blood Cell Suspensions Containing Gadolinium. J. Magn. Reson., 90:500.

[28] Koenig, S. H. 1991. From the Relaxivity of $Gd(DTPA)^{2-}$ to Everything Else. Magn. Reson. in Med., 22:183.

[29] Freed, J. H. 1978. Dynamic Effects of Pair Correlation Functions on Spin Relaxation by Translational Diffusion on Liquids: Finite Jumps and Independent $T_1$ Processes. J. Chem. Phys., 68:4034.

[30] Robertson, B. 1966. Spin-Echo Decay of Spins Diffusing in a Bounded Region. Phys. Rev., 151:273.

[31] Packer, K. J. 1973. The Effects of Diffusion Through Locally Inhomogeneous Magnetic Fields on Transverse Nuclear Spin Relaxation in Heterogeneous Systems. Proton Transverse Relaxation in Striated Muscle Tissue. J. Magn. Reson., 9:438.

[32] Nadler, W. and Schulten, K. 1985. Generalized Moment Expansion for Brownian Relaxation Processes. J. Chem. Phys., 82:151.

[33] Hahn, E. L. 1950. Spin Echos. Phys. Rev., 80:580.

[34] Torrey, H. C. 1956. Bloch Equations with Diffusion Terms. Phys. Rev., 104:563.

[35] Geraldes, C. F. G. C., Kuan, K. T., Koenig, S. H., Cacheris, W. P., Brown, III, R. D., Sherry, A. D., and Spiller, M. 1988. Magn. Reson. in Med., 8:191.

[36] Tilcock, C., Unger, E., Cullis, P., and MacDougall, P. 1989. Liposomal Gd-DTPA: Preparation and Characterization of Relaxivity. Radiology, 171:77.

[37] Swift, T. J. and Connick, R. E. 1962. NMR-Relaxation Mechanisms of $O^{17}$ in Aqueous Solutions of Paramagnetic Cations and the Lifetime of Water Molecules in the First Coordination Sphere. J. Chem. Phys., 37:307.

[38] Hirth, W. , October 1993, Mallinckrodt Co. (St. Louis, MO), personal communication.

[39] Crank, J. 1975. The Mathematics of Diffusion. Oxford Science Press, 2nd edition.

[40] Brünger, A., Peters, R., and Schulten, K. 1985. Continuous Fluorescence Microphotolysis to Observe Lateral Diffusion in Membranes: Theoretical Methods and Applications. J. Chem. Phys., 82:2147.

[41] Bauer, H.-U., Schulten, K., and Nadler, W. 1988. Generalized moment expansion of dynamic correlation functions in finite Ising systems. Phys. Rev. B, 38:445.

[42] Peters, R., Brünger, A., and Schulten, K. 1981. Continuous Fluorescence Microphotolysis: A New Method for the Study of Diffusion Processes in Single Cells. Proc. Nat. Acad. Sci. USA, 78:962.

[43] Barsky, D., Pütz, B., and Schulten, K. 1994. Diffusion Relaxation in Multi-Compartment Systems. In preparation.

[44] Stejskal, E. O. and Tanner, J. E. 1965. Spin Diffusion Measurements: Spin Echoes in the Presence of a Time-Dependent Field Gradient. J. Chem. Phys., 42:288.

[45] Tanner, J. E. and Stejskal, E. O. 1968. Restricted Self-Diffusion of Protons in Colloidal Systems by the Pulsed-Gradient, Spin-Echo Method. J. Chem. Phys., 49:1768.

[46] Stout, D. G. and Cotts, R. M. 1976. Measurement of Diffusional Water Permeability of Cell Membranes Using NMR without Addition of Paramagnetic Ions. In Resing, H. A. and Wade, C. G. (Eds.), Magnetic Resonance in Colloid and Surface Science, in *34*, 34, pages 31–35. American Chemical Society, Washington, D. C.

[47] Jr., R. F. K. and Lowe, I. J. 1980. A Modified Pulsed Gradient Technique for Measuring Diffusion in the Presence of Large Background Gradients. J. Magn. Reson., 37:75.

[48] Nayfeh, M. H. and Brussel, M. K. 1985. Electricity and Magnetism. John Wiley & Sons, New York.

[49] Albrand, J. P., Taieb, M. C., Fries, P. H., and Belorizky, E. 1983. NMR Study of SPectral Densities Over a Large Frequency Range for Intermolecular Relaxation in Liquids: Pair Correlation Effects. J. Chem. Phys., 78:5809.

[50] Hunter, J. R., Craig, P. D., and Philips, H. E. 1993. On the Use of Random Walk Models with Spatially Variable Diffusivity. J. Comp. Phys., 106:366.

[51] Pütz, B., Barsky, D., and Schulten, K. 1992. Edge Enhancement by Diffusion in Microscopic Magnetic Resonance Imaging. J. Magn. Reson., 97:27.

[52] Kennan, R. P., Zhong, J., and Gore, J. C. 1991. On the Relative Importance of Paramagnetic Relaxation and Diffusion-Mediated Susceptibility Losses in Tissues. Magn. Reson. in Med., 22:197.

[53] Hardy, P. and Henkelman, R. M. 1991. On the Transverse Relaxation Rate Enhancement Induced by Diffusion of Spins through Inhomogeneous Fields. Magn. Reson. in Med., 17:348.

[54] Muller, R. N., Gillis, P., Moiny, F., and Roch, A. 1991. Transverse Relaxivity of Particulate MRI Contrast Media: from Theories to Experiments. Magn. Reson. in Med., 22:178.

[55] Majumdar, S. and Gore, J. C. 1988. Studies of Diffusion in Random Fields Produced by Variations in Susceptibility. J. Magn. Reson., 78:41.

[56] Barsky, D., Pütz, B., Schulten, K., Schoeniger, J., Hsu, E. W., and Blackband, S. 1992. Diffusional Edge Enhancement Observed by NMR in Thin Glass Capillaries. Chem. Phys. Lett., 200:88.

[57] Walter, A., Lesieur, S., Blumenthal, R., and Ollivon, M. 1993. Size Characterization of Liposomes by HPLC. In Gregoriadis, G. (Ed.), Liposome Technology, Volume 1, chapter 16, pages 271–290. CRC Press, Boca Raton, Florida, 2 edition.

[58] Ye, R. and Verkman, A. S. 1989. Simultaneous Optical Measurement of Osmotic and Diffusional Water Permeability in Cells and Liposomes. Biochemistry, 28:824.

[59] Wayne, C. and Cotts, R. M. 1966. Nuclear Magnetic Resonance Study of Self-Diffusion in a Bounded Medium. Phys. Rev., 151:264.

[60] Turski, P., Kalinke, T., Strother, L., Perman, W., Scott, G., and Kornguth, S. 1988. MRI of Rabbit Brain after Intracarotiod Injection of Large Multivesicular Liposomes Containing Paramagnetic Metals and DTPA. Magn. Reson. in Med., 7:184.

[61] Josephson, L., Bigler, J., and White, D. 1991. The Magnetic Properties of Some Materials Affecting MR Images. Magn. Reson. in Med., 22:204.

[62] White, D. L., Aicher, K. P., Tzika, A. A., Kucharczyk, J., Engelstad, B. L., and Moseley, M. E. 1992. Iron-Dextran as a Magnetic Susceptibility Contrast Agent: Flow-Related Contrast Effects in the $T_2$-Weighted Spin-Echo MRI of Normal Rat and Cat Brain. Magn. Reson. in Med., 24:14.

[63] Lide, D. R. (Ed.) 1993. Handbook of Chemistry and Physics. CRC Press, Boca Raton, Florida, 74th edition.

## Footnotes

[1]It might be suggested that binding to plasma proteins should increase relaxivity, but it may also lead to dechelation of the agent, which, for $Gd(DTPA)^{2-}$, would be toxic.

[2]The transverse magnetization can be described in exactly the same way if one applies a transformation $m_{\text{trans}}(\vec{r},t) = e^{-i\omega_0 t} m(\vec{r},t)$ which is valid in the absence of non-discountable (via spin-echo, etc.) field inhomogeneities. Such non-discountable inhomogeneities will occur in the case of superparamagnetic contrast agents and, to a lesser extent, due to susceptibility effects outside of Gd-filled vesicles. $T_1$-weighted images will minimize these latter effects.

[3]We use the simplification $V_f = \frac{r_1^3}{r_3^3 - r_1^3} \overset{V_f \ll 1}{\simeq} \left(\frac{r_1}{r_3}\right)^3$ which introduces an error of less than 1% for the systems considered here, where $V_f \lesssim 0.01$.

[4]Including the native relaxation in the description would merely contribute the corresponding rate $R_{\text{native}}$ to the diagonal elements of the rate matrix $\mathcal{R}$ in Eq. (6).

[5]In this respect, the model we employ in our simulations differs slightly from [10] in that we calculate $(\delta\omega)^2$ on the outer membrane surface rather than at the inner surface. Thus, we introduce a dependence of $(\delta\omega)^2$ on the liposome radius as shown in Table 1.

[6]By field cycling relaxometry, these mechanisms can in some cases be distinguished [10].

FIG 1: Model of the liposome system. The radii $r_1, r_2$, and $r_3$ characterize the inside and outside radii of the liposome membrane and the radius of the average volume per liposome, respectively. In region I relaxation is enhanced by the contrast agent, and in region II (the membrane and the outside) the relaxation takes place at the native rate. Exchange pathways, characterized by the exchange rates $R_{\mathrm{io}}$ and $R_{\mathrm{oi}}$, between region I and region II are indicated by thick arrows.

FIG 2: Dipole field $B_z$ in region II, rescaled for each liposome radius $r_1$ such that the ratio $r_1/r_3 = \sqrt[3]{V_f}$ is held constant for $V_f = 0.003$. The liposome interior, region I, is shown as the gray circle in the center. Assuming a constant membrane thickness $d$=5 nm, the membrane appears proportionally thicker for smaller liposomes; the membrane for a 70 nm liposome is indicated by the white ring around region I, while the membrane for a 400 nm liposome is depicted by the thick line bounding region I.

FIG 3: Weighted susceptibility (in ppm) of a $\mathrm{Gd(DTPA)}^{2-}$ solution, calculated from Eq. (42), versus $\mathrm{Gd(DTPA)}^{2-}$ [mM] concentration. The upper, solid curve corresponds to a 670 mM solution of $\mathrm{Gd(DTPA)}^{2-}$ where 257 mL of water are displaced per mole of $\mathrm{Gd(DTPA)}^{2-}$. For reference, the lower, dashed curve assumes no water is displaced by the $\mathrm{Gd(DTPA)}^{2-}$. The susceptibility of the water surrounding the liposome is indicated by the dot-dashed line. The two points (•) indicate the concentrations for which the water displacement has been measured [38].

FIG 4: Permeability (from Eq. 16) as a function of mean outer diameter for egg PC/cholesterol=6/4 liposomes with internal relaxation rates of 1869 Hz (data from [36]). The horizontal line corresponds to 16 $\mu$m/s. The error bars are due to the uncertainty in the liposome sizes.

FIG 5: Relaxation rate enhancement $1/T_{\mathrm{para}}$ as a function of mean outer diameter for liposomes of relative abundance $V_f = 0.003$ with, respectively, internal relaxation rates and permeabilities of: (dashed line) 420 Hz, 8.7 $\mu$m/s and (solid curve) 1869 Hz, 16 $\mu$m/s. (The last value is derived from 16.) The data points are for egg PC/cholesterol=6/4 liposomes (•) in [36] and (○) in [25]), where the latter datum has been recalculated for the same $V_f$. Also shown (wide dashes) is $1/T_{\mathrm{para}}$ for an internal rate of 420 Hz and permeability of 136 $\mu$m/s.

FIG 6: Relaxation rate enhancement as a function of mean outer diameter. The solid curve corresponds to that of Fig. 5. Also plotted are the corresponding rates for Gaussian distributions of liposomes with standard deviations of 20 nm (with a lower diameter limit set physically at 25 nm) (short dashed line), and the rates as a function of diameter reduced by 3/10 (wide dashes).

FIG 7: Computer simulation results of outer sphere relaxation rate versus echo time $\tau_H$ for liposomes of 100 nm (○), 200 nm (○) and 400 nm (●) outer diameter filled with 670 mM Gd(DTPA)$^{2-}$ solution in a static field of 1.5 T. The liposomes occupied 0.3 % of the total volume. The echo time $\tau_R$, the upper bound for the $t^2$ region, is indicated by ↓ symbols for 200 and 400 nm liposomes. For 100 nm $\tau_R$ is just off the left edge of the plot. The times $\tau_D$, related to reaching the asymptotic relaxation rate, is indicated by ↑ symbols.

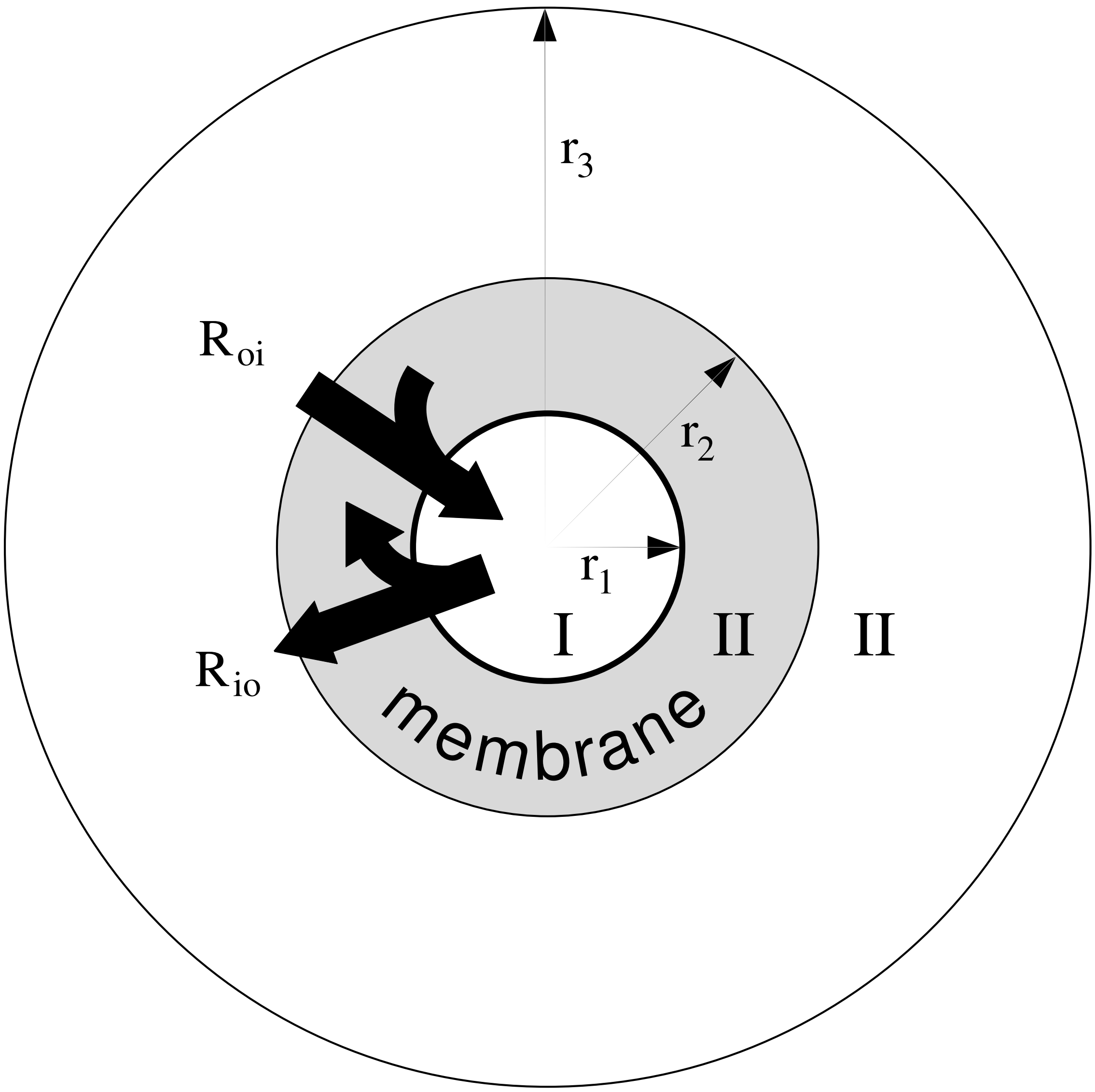

r3
R oi
r2
r1
I
II
II
R io
membrane

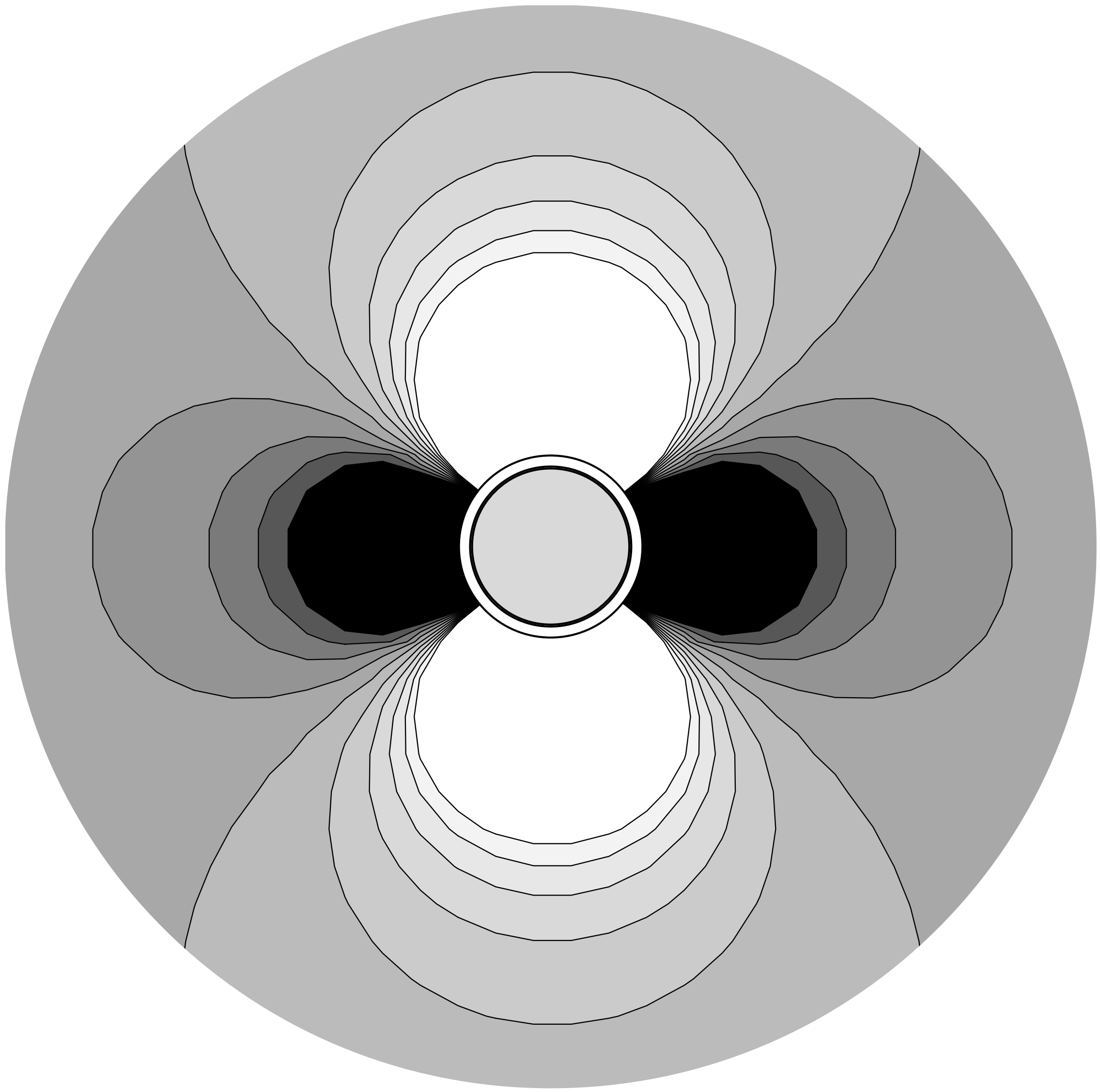

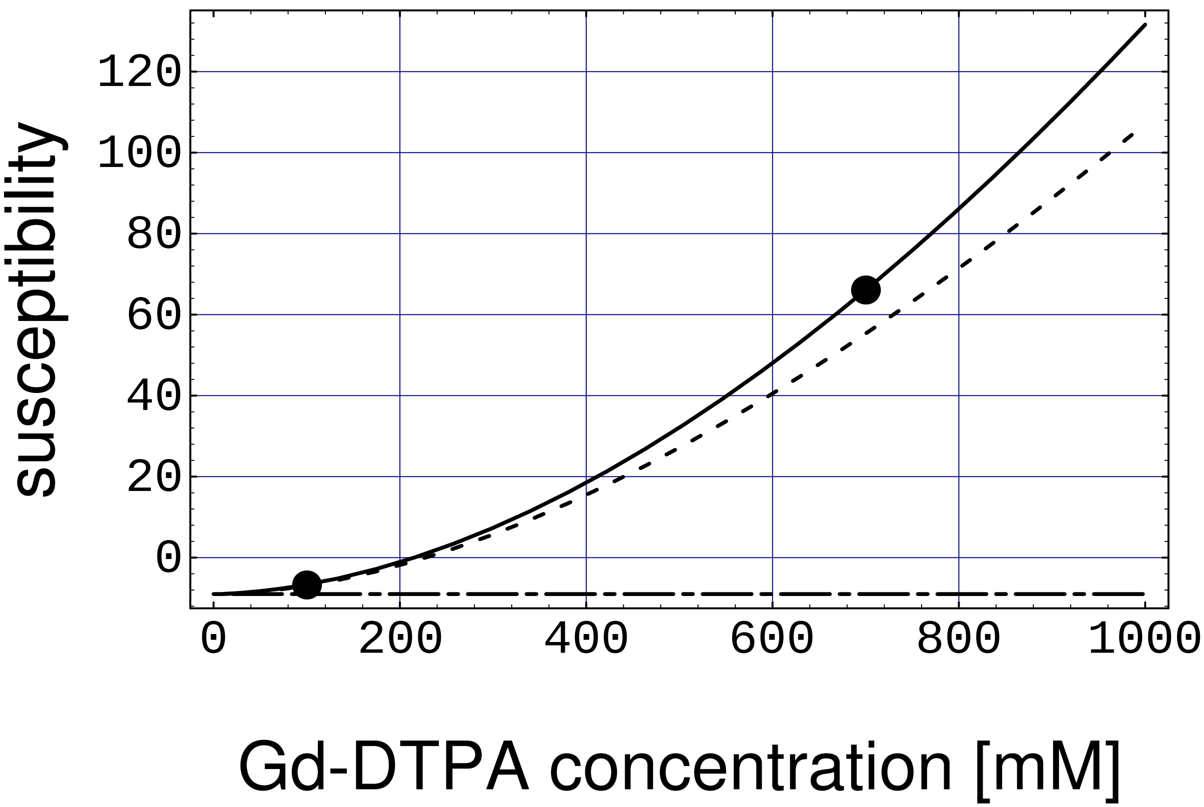

susceptibility
120
100
80
60
40
20
0
0
200
400
600
800
1000
Gd-DTPA concentration [mM]

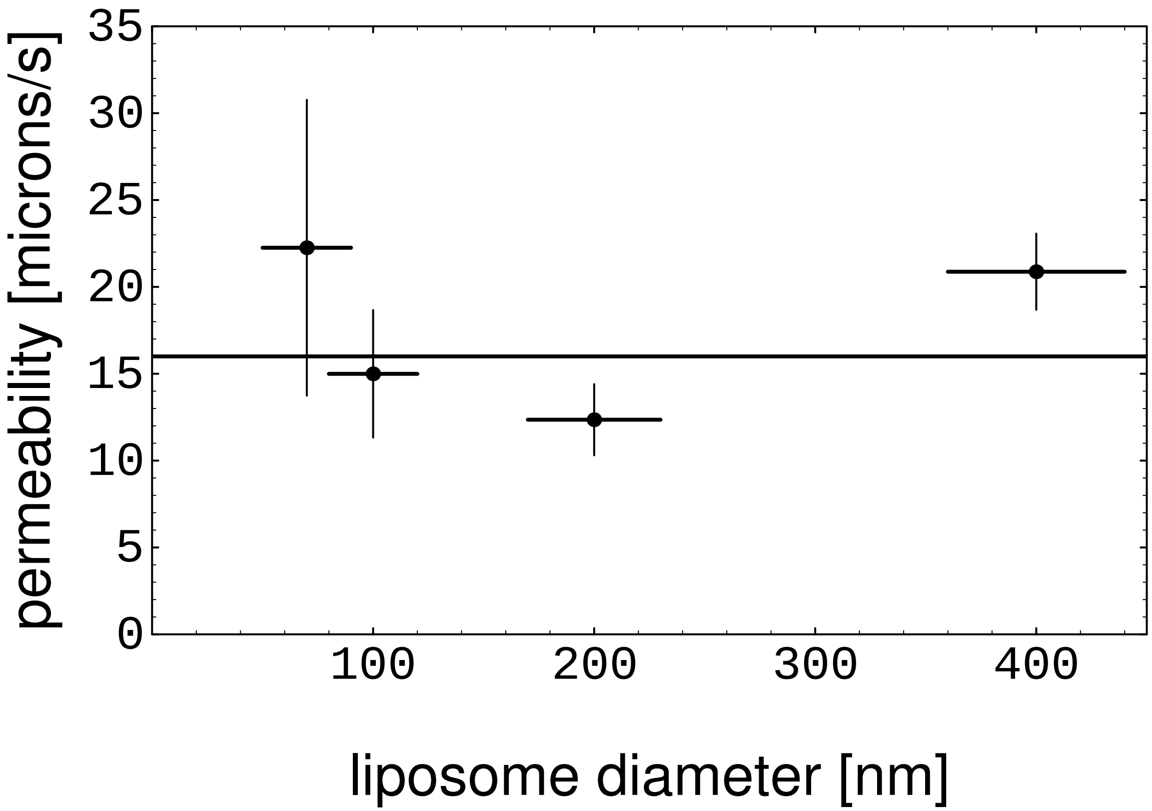

permeability [microns/s]
35
30
25
20
15
10
5
0
100
200
300
400
liposome diameter [nm]

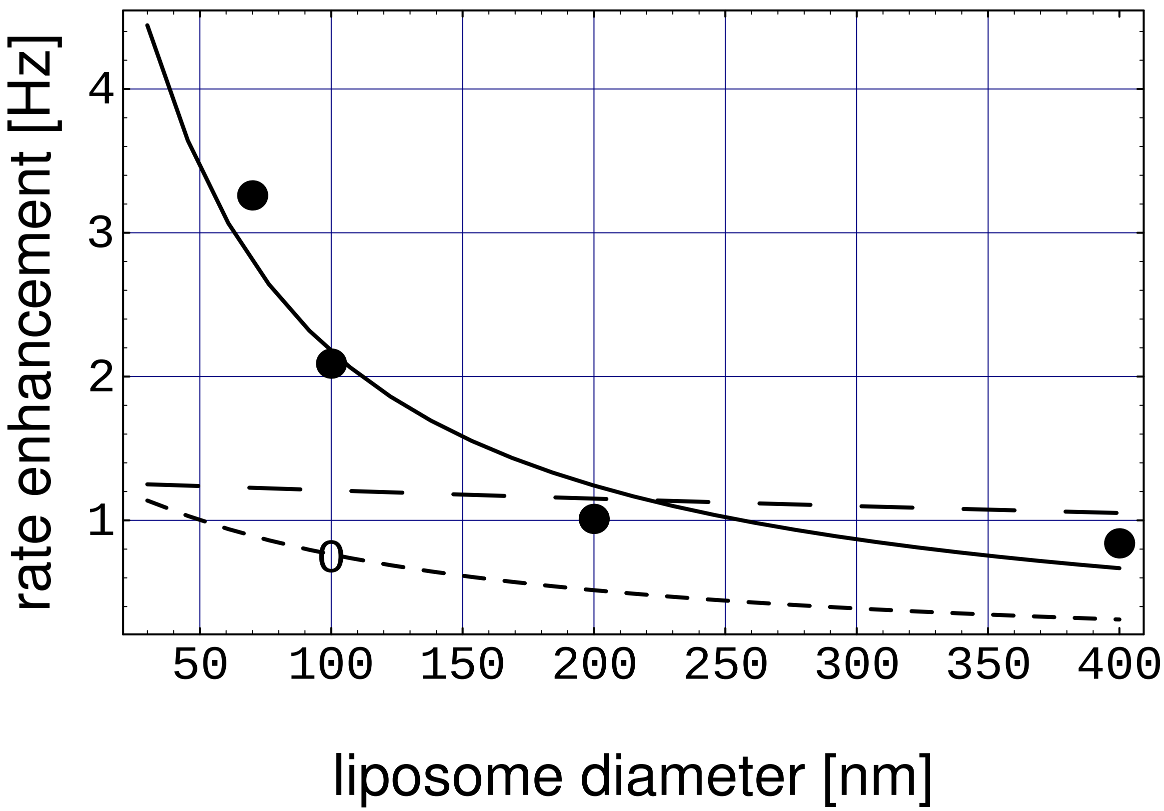

rate enhancement [Hz]
4
3
2
1
0
50
100
150
200
250
300
350
400
liposome diameter [nm]

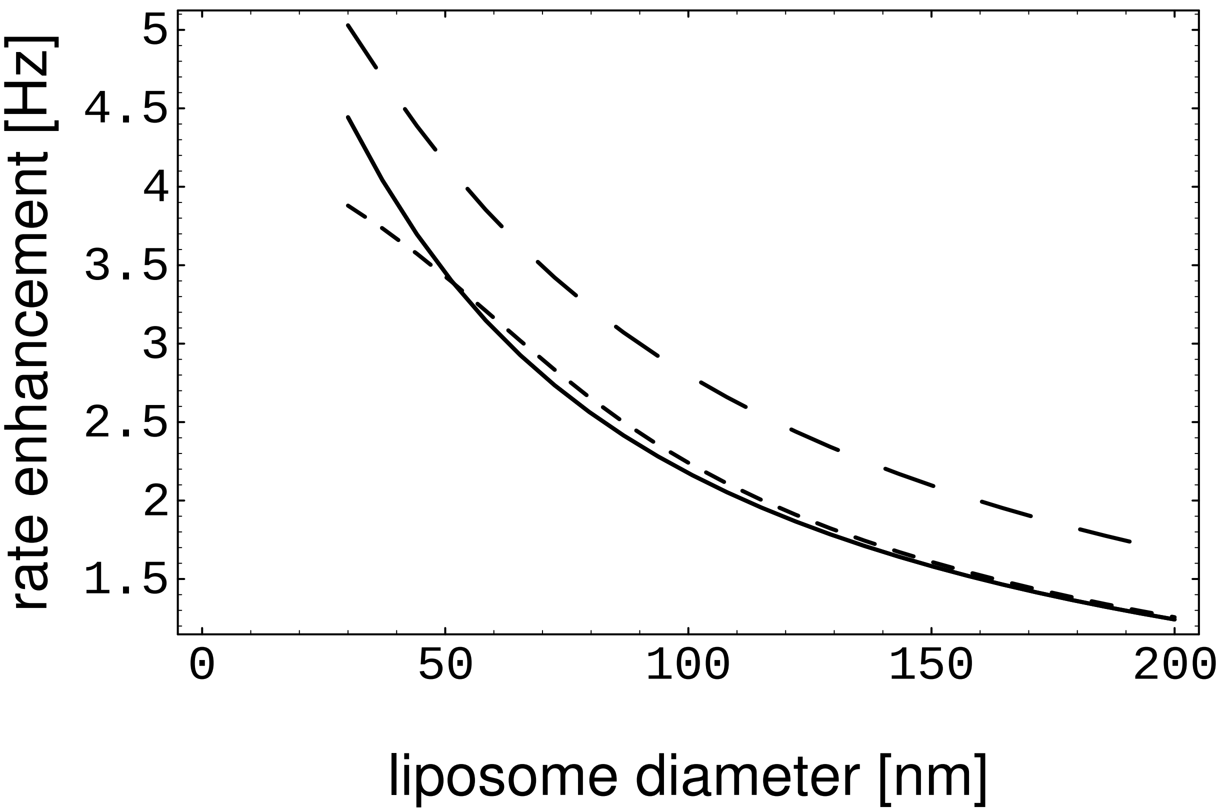

rate enhancement [Hz]
5
4.5
4
3.5
3
2.5
2
1.5
0
50
100
150
200
liposome diameter [nm]

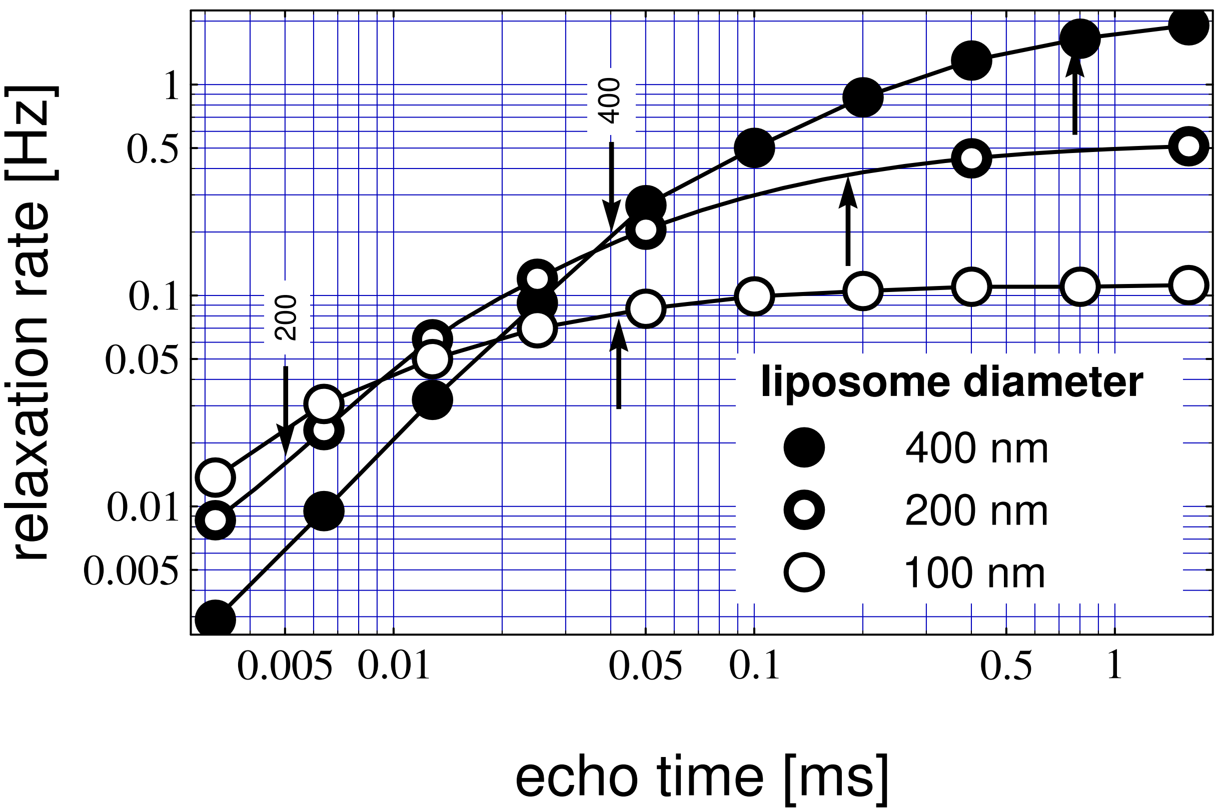

relaxation rate [Hz]
1
0.5
0.1
0.05
0.01
0.005
0.005
0.01
0.05
0.1
0.5
1
echo time [ms]
400
200
liposome diameter
400 nm
200 nm
100 nm